Geological Society of America
Special Paper 402
2006

New Sr-Nd-Pb-O isotope data for Colima volcano and evidence for the nature of the local basement

Gabriel Valdez-Moreno[†]
Posgrado en Ciencias de la Tierra, Instituto de Geofísica, Universidad Nacional Autónoma de México (UNAM), México, D.F., Mexico

Peter Schaaf
Laboratorio Universitario de Geoquímica Isotópica (LUGIS), Instituto de Geofísica and Instituto de Geología, Universidad Nacional Autónoma de México (UNAM), México, D.F., Mexico

José Luis Macías
Departamento de Vulcanología, Instituto de Geofísica, Universidad Nacional Autónoma de México (UNAM), México, D.F., Mexico

Minoru Kusakabe
Institute for Study of the Earth's Interior, Okayama University, Misasa, Tottori-ken 682-0193, Japan

ABSTRACT

Colima volcano is situated at the western edge of the Mexican volcanic belt within the Colima rift zone. This contribution presents new geochemical and Sr-Nd-Pb-O isotope data for Colima volcano rocks and plutonic xenoliths found in prehistorical lava flows. Colima volcano magmas display strong subduction signatures (positive peaks of Ba, K, Pb, and Sr, and negative anomalies of Nb and Ti) and were generated in a depleted mantle source and emplaced at crustal levels (garnet-free zone), where they experienced fractional crystallization of plagioclase and pyroxene. Gabbroic and granitoid xenoliths found in prehistorical lava flows show evidence for partial melting and are considered to be representative of the basement beneath Colima volcano. At upper-crustal levels, Colima volcano magmas were contaminated by granitoids, like those of the nearby Cretaceous Manzanillo and Jilotlán Batholiths. Sr-Nd isotope ratios of these intrusives are nearly identical to those of Colima volcano lavas. For that reason assimilation of the granitic crust is not detectable in diagrams of these isotopic systems but can be clearly seen in a ε_{Nd} versus $\delta^{18}O$ plot. In comparison to other large Mexican volcanic belt stratovolcanoes, Colima volcano lavas display the least evolved geochemical and isotopic signatures of this arc.

Keywords: Colima volcano, Mexican Volcanic Belt, isotope geochemistry, crustal contamination, xenoliths.

[†]E-mail: valdezm@servidor.unam.mx.

Valdez-Moreno, G., Schaaf, P., Macías, J.L., and Kusakabe, M., 2006, New Sr-Nd-Pb-O isotope data for Colima volcano and evidence for the nature of the local basement, *in* Siebe, C., Macías, J.L., and Aguirre-Díaz, G.J., eds., Neogene-Quaternary continental margin volcanism: A perspective from Mexico: Geological Society of America Special Paper 402, p. 45–63, doi: 10.1130/2006.2402(02).

INTRODUCTION

Colima volcano (3850 m above sea level [a.s.l.]), located 30 km north of the city of Colima, is considered to be the most active volcano of the Mexican volcanic belt and North America (Luhr and Carmichael, 1980; Medina, 1983; De La Cruz-Reyna, 1993; Robin and Potrel, 1993; Saucedo and Macías, 1999; Bretón-González et al., 2002; Carmichael, 2002; Luhr, 2002; Saucedo et al., 2004). Colima volcano, also known as Volcán de Fuego, represents the youngest edifice of the Colima volcanic complex, a volcanic chain formed by three N-S–oriented andesitic stratovolcanoes and alkaline scoria cones (Fig. 1; Cortés-Cortés et al., 2005). The magmatism of Colima volcano has been related to the subduction of the Cocos and Rivera plates beneath the North America plate (Fig. 1; Luhr and Carmichael, 1980; Hochstaedter et al., 1996). However, extensive discussion exists regarding the position of the Rivera and Cocos plate boundary in front of the Colima rift zone (Fig. 1; Bandy et al., 1995). Colima volcano is located only ~150 km NE of the Middle America Trench, thus being the closest volcano of the Mexican volcanic belt to the trench.

The generation of contemporary subalkaline magmas (stratovolcanoes) and alkaline magmas (cinder cones) at the Colima volcanic complex has been attributed to the superposition of subduction and rifting tectonic regimes (Allan and Carmichael, 1984; Allan, 1986; Luhr and Carmichael, 1990; Luhr, 1997).

The historical record of Colima volcano shows two major explosive eruptions in 1818 and 1913. The latter event established a 21-km-high eruptive column, which generated ash fall as far as the city of Saltillo, located 725 km northeast of the crater (Saucedo, 1997). During the last six years, the volcanic activity has been characterized by the formation of domes, lava flows, pyroclastic flows, and dome explosion events (Smithsonian Institution, 2002).

Several studies have been published on different aspects of the Colima volcanic complex, mainly focusing on the recent eruption cycle (Rodríguez-Elizarrarás et al., 1991; Saucedo and Macías, 1999; Saucedo et al., 2002), magmatic processes (Robin et al., 1987; Luhr, 2002; Mora et al., 2002), geochemistry (Luhr and Carmichael, 1980, 1982; Robin et al., 1987; Macías et al., 1993; Luhr, 2002; Mora et al., 2002), and isotopic compositions (Moorbath et al., 1978; Carmichael and DePaolo, 1980; Verma and Luhr, 1993; Wallace and Carmichael, 1994; Luhr, 1997; Taran et al., 2002).

Regarding the last set of studies, Carmichael and DePaolo (1980) presented $^{87}Sr/^{86}Sr$ and ε_{Nd} data for Colima volcano and

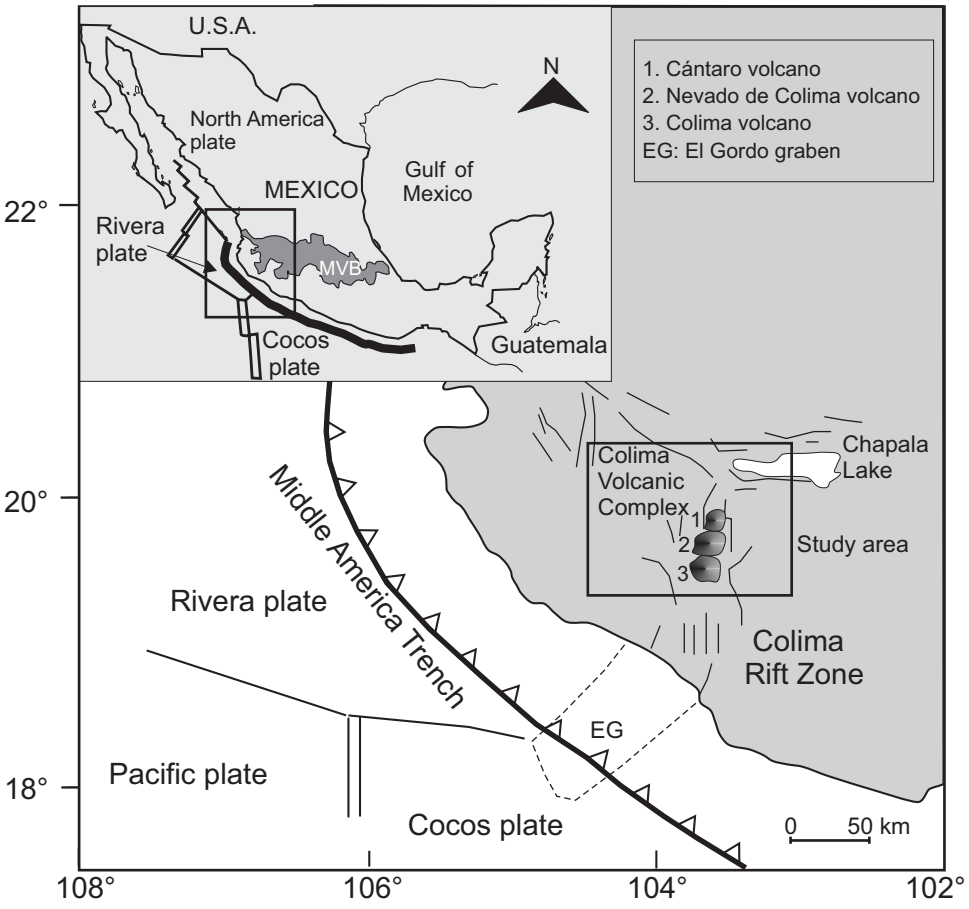

Figure 1. Location of the Mexican volcanic belt (MVB), the Colima volcanic complex in the Colima rift zone, the Middle America Trench (thick line in inset), and additional tectonic features in western Mexico.

the surrounding alkaline cinder cones that range from 0.7035 to 0.7039 and from +6 to +3, respectively. They interpreted these isotope data as indicative of magmas derived from crust beneath island arcs or from a heterogeneous mantle. Moorbath et al. (1978) presented eight Sr isotope analyses from Colima volcanic complex andesites and suggested that the low $^{87}Sr/^{86}Sr$ ratios (0.7035–0.7040) reflected an insignificant sialic contribution to their origin. Verma and Luhr (1993) reported Sr, Nd, and Pb isotope data for three samples from the 1913 and 1982 eruptions and proposed that calc-alkaline andesites of the Colima volcano were derived from a less radiogenic strontium source, or had undergone a lower degree of crustal contamination, in comparison to other andesites from the Mexican volcanic belt. In a preliminary stable isotope study, Taran et al. (2002) showed that hornblendes from Colima volcano are enriched in deuterium (δD from –17‰ to –15‰). The high δD values probably represent magmatic water in andesites from subduction-influenced settings. The combination of stable and radiogenic isotopic studies (e.g., $\delta^{18}O$ versus $^{87}Sr/^{86}Sr$) is particularly important, since it has been demonstrated to be a powerful tool for characterizing magmatic processes, such as crustal contamination (Taylor, 1980; James, 1981; Chivas et al., 1982; Eiler et al., 2000; Vroon et al., 2001; Hansteen and Troll, 2003; Bindeman et al., 2004).

In this work, we present new $\delta^{18}O$ data combined with Sr, Nd, and Pb isotopes on prehistorical and historical products of Colima volcano. We discuss the role of crustal contamination and other magmatic processes on the genesis of the andesitic rocks. We also contribute some new information on the nature of the continental crust beneath Colima volcano.

GEOLOGICAL SETTING

Colima volcano forms part of the Colima volcanic complex, which is a N-S–aligned volcanic chain located inside the Colima rift zone (Fig. 1). The northernmost and oldest edifice is the dacitic-andesitic Cántaro volcano (2900 m above sea level [a.s.l.], K-Ar whole rock and hornblende ages from 1.7 Ma to 0.6 Ma; Allan [1986]). Further to the south, the andesitic Nevado de Colima volcano (4260 m a.s.l.) initiated its activity at ca. 0.53 Ma (Robin et al., 1987) and was active until ca. 8000 yr B.P. (Robin et al., 1990).

Robin et al. (1987) interpreted the caldera rim on the northern flank of Colima volcano, emplaced farthest south, as a rem-

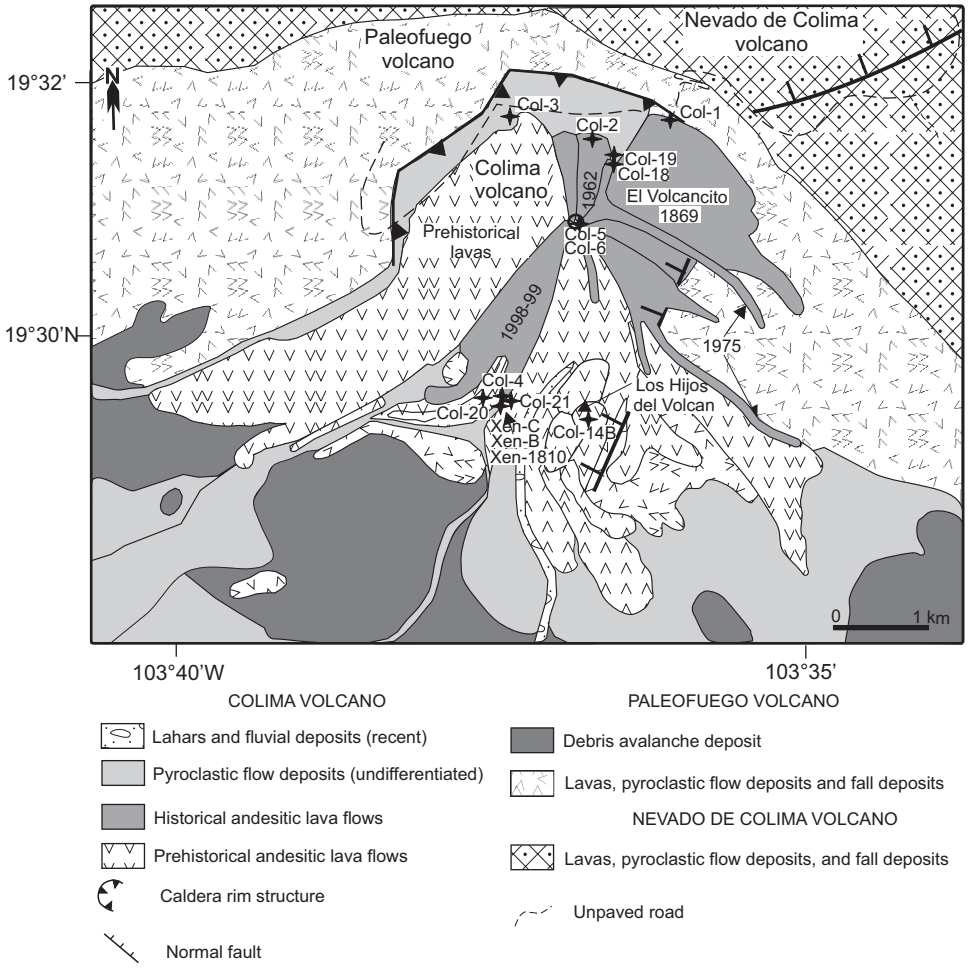

Figure 2. Geological sketch map of Colima volcano, modified from Rodríguez-Elizarrarás (1995), Luhr (2002), and Cortés-Cortés et al. (2005) with the distribution of some historical lava flows. Stars and numbers indicate sample locations.

nant feature of a volcanic collapse of the primitive volcano, which they called Paleofuego, dated at 9370 ± 400 yr B.P. However, Luhr and Prestegaard (1988) proposed a younger age for this event of 4280 ± 110 yr B.P., and Komorowski et al. (1993) suggested an even younger age for the collapse. Colima volcano (3850 m a.s.l.) was emplaced inside the horseshoe-shaped caldera rim of Paleofuego volcano. The exact age of its formation is still unknown, and the oldest historical activity (1560 A.D.) is reported in Medina (1983) and De La Cruz-Reyna (1993). Maps of the Colima volcanic complex were published by Rodríguez-Elizarrarás (1995), Luhr and Carmichael (1990), and Cortés-Cortés et al. (2005), and a simplified map of Colima volcano is presented in Figure 2.

Geophysical investigations indicate that the crustal basement beneath Colima volcano has a thickness of 28–35 km and is of a granitic-granodioritic nature (Urrutia-Fucugauchi and Molina-Garza, 1992; Bandy et al., 1995; Urrutia-Fucugauchi et al., 1999).

Colima volcano is partially surrounded by Cretaceous limestones of the Tepames Formation (Smith, 1990), which is extensively intruded by plutonic rocks (Fig. 3). The Manzanillo Batholith, exposed to the southwest of Colima volcano, is composed of granodiorites and gabbros (Fig. 3; Rb-Sr isochron age of 69 ± 3 Ma; Rb-Sr and K-Ar biotite and hornblende cooling ages 59.1–69.5 Ma), and tonalites and gabbros of the Jilotlán Batholith are exposed to the east of Colima volcano (Fig. 3; Rb-Sr isochron age of 68 ± 12 Ma; Rb-Sr and K-Ar biotite and hornblende cooling ages 55.2–60.3 Ma; Schaaf [1990]). A granodiorite stock 45 km north of Cántaro volcano yielded a K-Ar biotite cooling age of 69.43 ± 1.14 Ma (Allan, 1986). Allan and Carmichael (1984) described the presence of granitic xenoliths up to 15 cm long in the phlogopite-bearing lamprophyres in the Colima graben walls.

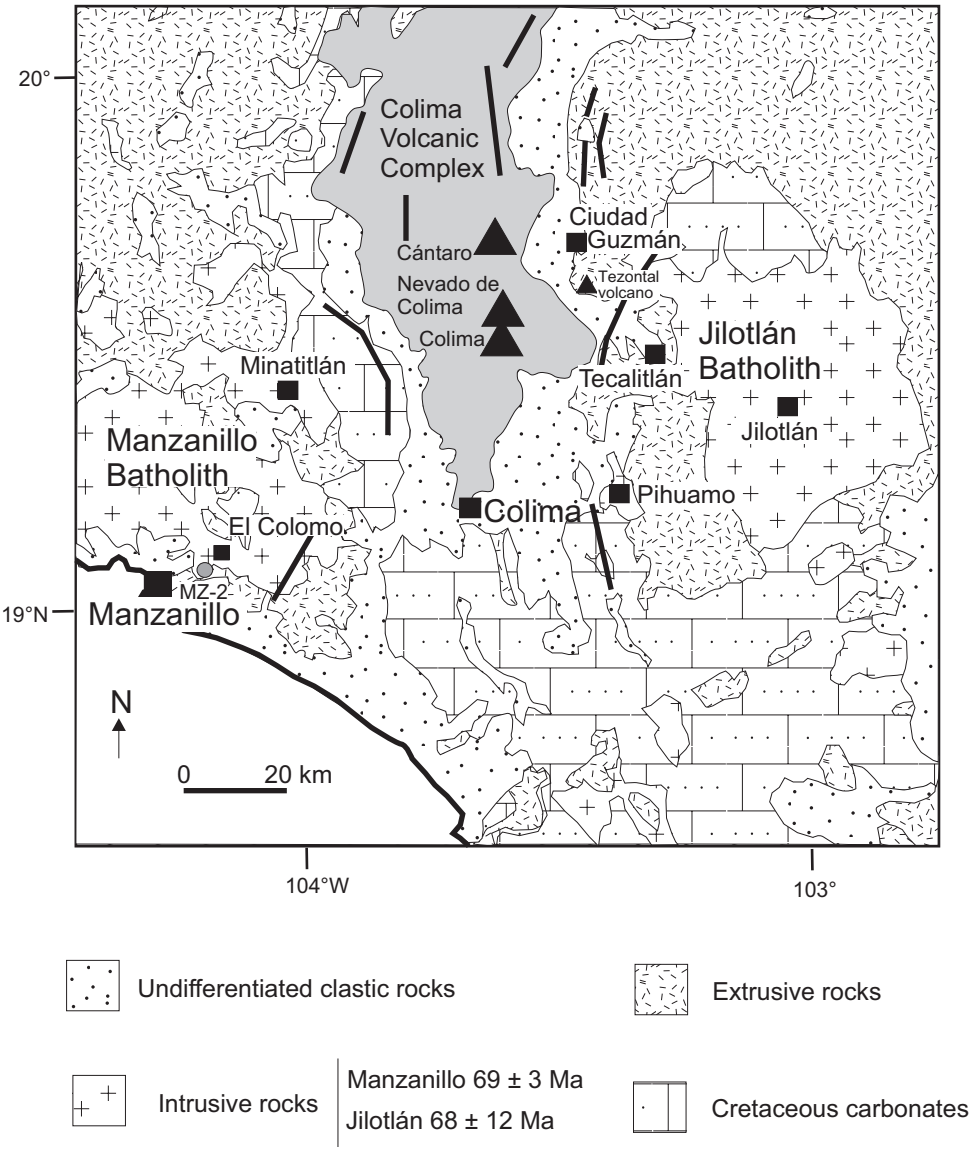

Figure 3. Simplified regional geological map showing the location of Colima volcano and the Manzanillo and Jilotlán Batholiths. Filled squares are main cities and towns. Location of sample MZ-2 is also shown. Black lines represent major faults. Figure is modified from Bandy et al. (1995).

SAMPLE COLLECTION

A total of 17 samples were collected from Colima volcano, together with a granodioritic sample from the Manzanillo Batholith (MZ-2). These samples are: three prehistorical lava flows previously described by Luhr and Carmichael (1980) from the northern and southern Colima volcano slopes, four lavas from the 1869, 1962, 1975, and 1998 events, a dome sample from Los Hijos del Volcán on the southern flank of Colima volcano, two pumice samples from historical (probably) 1818 and 1913 Plinian fallouts, one scoria fragment from the 1913 pyroclastic flow deposit, the November 2001 crater spine, and the January-February 2002 dome. Additionally, we sampled three xenoliths (one microgabbro and two granodiorites) hosted in prehistorical andesitic lava flows on the southern flank of Colima volcano. Sample locations are shown in Figure 2 (Colima volcano) and Figure 3 (MZ-2), and sample coordinates are given in Table 1.

PETROGRAPHY

Eleven samples were studied in detail under the petrographic microscope.

Andesitic rocks (lavas, pumice, scoria, and dome samples) of Colima volcano are densely porphyritic (24–50 vol% phenocrysts; Table 2) with a mineral assemblage represented by plagioclase + pyroxene (augite + hypersthene) ± hornblende ± Fe-Ti oxides, and accessory apatite. These minerals are set in a pilotaxitic to hyalopilitic matrix composed of brown glass and microlites of the same minerals. Hornblende was not observed in the matrix, as previously reported by Luhr and Carmichael (1980).

Prehistorical and historical lavas show ~1.5 mm olivine xenocrysts, frequently mantled by reaction rims composed of symplectitic titanomagnetite, pyroxene, and plagioclase. These observations confirm the findings of Luhr (2002) in historical lavas. The hornblende-rich dome sample Col-14B (Los Hijos del Volcán) shows accumulation of aggregates composed of up to 2 mm augite crystals and evidence of intensely melted clinopyroxene, replaced by brown glass and plagioclase. Sample Col-20 shows two zones with different contents of brown glass: a glass-rich zone with corroded plagioclase rims and a zone with less abundant glass and uncorroded plagioclase (Fig. 4A). Some plagioclase crystals show sieve textures with brown glass inclusions and dusty corrosion rims. Reddish hornblende (oxyhornblende) is a common phase in Col-14B and Col-21 (lava) samples. Hornblende has dark reaction rims composed of fine-grained magnetite (opacite), pyroxene, and plagioclase. Sometimes hornblende presents inclusions of pyroxene, resulting in a poikilitic texture.

Several petrological studies on historical lavas have been carried out (Luhr and Carmichael, 1980; Robin et al., 1987; Luhr, 2002; Mora et al., 2002). These studies have pointed out a decreasing trend of hornblende contents from older to modern eruptions. The other mineral phases (plagioclase + augite + hypersthene ± Fe-Ti oxides and apatite) are present in lavas of all ages.

Sample Col-20 of the andesitic prehistorical lavas exposed on the southern flank of Colima volcano contains 1–2-cm-long xenoliths. They show quenched textures with randomly oriented, interlocking columnar or acicular crystals of plagioclase + orthopyroxene ± hornblende, with brown interstitial glass and vesicles (Fig. 4B). The rims of these xenoliths show evidence of melting, abundant brown glass, and sieve-textured plagioclase crystals.

The gabbroic xenolith (Xen-B; plagioclase + clinopyroxene + orthopyroxene + titanomagnetite + glass ± hornblende) displays evidence of partial melting of clinopyroxene, where large crystals are replaced by short tabular plagioclase and brown glass. Throughout the xenolith, veins of brown glass are commonly present together with tabular plagioclase crystals (Fig. 4C).

Pink to light-green, 5–15-cm-long porous xenoliths (e.g., samples Xen-C and Xen-1810) were found in scoriaceous andesitic prehistorical lavas of Colima volcano. They have rounded to angular borders with the host rock (Fig. 5A–B). These xenoliths have a microgranular texture and, together with the remnant mineralogy, a plutonic origin is suggested. The mineral association is plagioclase + pyroxene ± K-feldspar >> quartz and glass, and vesicles are present (which is discussed later in detail).

Sample Xen-1810 is vesicular and contains abundant colorless to pale-brown glass. Quartz is rare and frequently shows intense melting resulting in the formation of pale-pink glass, irregular borders, and embayments (Fig. 5C–D). Microcline crystals, displaying corroded borders and typical twinning bars, are also present. The remnant mineralogy suggests that the original rock was an intermediate to felsic intrusive rock, possibly of granodioritic composition.

In conclusion, clinopyroxene phenocrysts in the xenoliths are often intensely corroded and show fritted textures together with the accumulations of short tabular plagioclase crystals. Interstitial colorless to pink glass in quartz could be interpreted as the result of partial melting due to reheating of the xenoliths as documented by Harris and Bell (1982), Heliker (1995), and Costa et al. (2002) in xenoliths from Ascension Island (South Atlantic), Mount St. Helens (USA), and San Pedro volcano (Chile).

ANALYTICAL METHODS

A total of 3–4 kg of rock sample and ~100–300 g of xenoliths, previously examined for freshness, were broken in a jaw crusher, aliquotized, and finally pulverized with a steel mill set.

Chemical analyses were obtained using several analytical techniques. Whole-rock major-element concentrations were determined via X-ray fluorescence on fused glass disks. These were prepared by mixing dry sample powder with $Li_2B_4O_7$-$LiBO_2$ flux mixture (50:50 wt%), with melting achieved in Pt crucibles. Major elements were analyzed with a sequential Siemens SRS3000 spectrometer at the Laboratorio Universitario de Geoquímica Isotópica (LUGIS, Instituto de Geología, Universidad Nacional Autónoma de México [UNAM]). The calibration curves were performed using 35 international reference standards. In another set of samples, major-element concentrations

TABLE 1. MAJOR (WT%) AND TRACE-ELEMENT (PPM) ANALYSES OF PREHISTORICAL AND HISTORICAL LAVAS, SCORIA, DOMES, AND XENOLITHS FROM COLIMA VOLCANO AND A GRANODIORITE SAMPLE FROM THE MANZANILLO BATHOLITH

	Pre-historical lavas				Historical lavas								
Sample	Col-19	Col-14B	Col-20	Col-21	*Col-1	*Col-2	*Col-3	*Col-4	**Col-5	**Col-6	*Col-9	*Col-12	Col-18
Location	North slopes	Los Hijos del Volcan	South flank	South flank	El Volcancito	El Playón	El Playón	El Cordobán	Dome-Crater	Dome-Crater	Nevado-slopes	San Antonio	North slopes
Rock type	Lava	Dome	Lava	Lava	Lava	Lava	Scoria	Lava	Spine dome	Dome	Pumice	Scoria fragment	Lava
Mineralogy	Plg>px> Fe-Ti oxides	Plg>hbl>px> Fe-Ti oxides	Plg>px> Fe-Ti oxides	Plg>px> hbl	Plg>hbl>px >Fe-Ti oxides	Plg>px> Fe-Ti oxides>hbl	Plg>px>hbl> Fe-Ti oxides	Plg>px>hbl >Fe-Ti oxides	Plg>px> Fe-Ti oxides	Plg>px> Fe-Ti oxides	Plg>px>hbl Fe-Ti oxides	Plg>px> Fe-Ti oxides>hbl	Plg>px>hbl> Fe-Ti oxides
Eruption date	pre-historical lavas	pre-historical	pre-historical	pre-historical	1869	1962	1913	1998	2001	2002	1818	1913	1975
Latitude N	19°31′15″	19°29′55″	19°29′28″	19°29′19″	19° 31′35″	19° 31′26″	19°31′ 40″	19°29′29″	19°30′ 50″	19°30′ 50″	19°35′4″	19°27′11″	19°29′54″
Longitude W	103°36′43″	103°37′ 42″	103°37′44″	103°07′25″	103° 36′20″	103°37′4″	103°37′ 29″	103°37′31″	103°37′ 02″	103°37′ 02″	103°35′54″	103°42′49″	103°37′08″
Major oxides (wt%)													
SiO_2	58.05	60.58	58.17	58.72	60.67	60.32	58.20	59.68	60.09	59.93	58.14	58.79	61.42
TiO_2	0.78	0.58	0.64	0.65	0.580	0.649	0.750	0.638	0.66	0.625	0.664	0.667	0.61
Al_2O_3	17.86	17.47	17.45	17.98	17.84	17.54	17.38	17.27	16.14	17.57	17.62	17.31	17.60
Fe_2O_3 (t)	6.59	6.21	6.16	6.32	5.56	5.93	6.62	6.07	6.22	5.97	6.06	6.41	5.76
MnO	0.13	0.12	0.11	0.12	0.103	0.105	0.115	0.105	0.12	0.150	0.107	0.110	0.11
MgO	4.17	3.50	3.44	3.84	2.76	3.04	4.07	3.89	4.03	3.93	3.83	4.53	2.83
CaO	7.04	6.11	6.21	6.45	5.85	5.95	6.81	6.22	6.23	6.32	6.47	6.67	5.92
Na_2O	4.39	4.56	4.36	4.44	4.82	4.72	4.48	4.62	4.98	4.34	4.57	4.28	4.74
K_2O	1.26	1.16	1.38	1.13	1.57	1.43	1.24	1.33	1.32	1.25	1.20	1.07	1.39
P_2O_5	0.23	0.17	0.24	0.17	0.22	0.21	0.20	0.20	0.20	0.19	0.18	0.17	0.21
L.O.I.	–0.04	0.00	1.99	0.13	0.03	–0.07	0.09	–0.15	–0.02	0.03	0.33	0.12	–0.09
SUM	100.46	100.46	100.16	99.94	100.00	99.82	99.96	99.87	99.97	100.30	99.17	100.13	100.50
Trace elements (ppm)													
Ni	20.0	29.6	24.3	54.9	21.2	26.1	32.1	43.1	32.0	na	176.0	54.5	20.0
V	116.0	91.6	121.1	127.6	98.8	113.0	151.5	131.6	90.0	na	133.1	148.0	83.8
Cr	140.8	182.6	179.4	168.4	147.1	142.7	194.0	225.6	70.0	na	175.2	241.2	116.1
Co	16.4	14.6	15.5	18.1	11.8	14.2	19.4	18.9	15.0	na	18.8	21.6	12.5
Cu	20.8	17.3	21.6	34.0	19.8	23.6	30.3	34.4	19.0	na	83.9	31.1	22.0
Zn	71.3	66.9	89.5	83.1	125.0	70.3	78.2	75.0	135.0	na	74.0	81.3	82.3
Ga	17.8	17.5	18.3	17.9	19.4	19.2	20.6	21.2	na	na	18.8	20.4	18.1
Ge	1.10	1.17	1.50	1.46	1.19	1.27	1.34	1.37	na	na	1.04	1.23	1.15
Rb	16.1	16.8	19.8	17.5	20.3	20.9	17.8	21.1	17.8	na	17.4	17.1	20.4
Sr	615.8	502.3	731.4	537.7	630.4	571.0	658.5	648.3	551.0	na	597.6	602.4	535.8
Y	17.05	14.90	16.05	16.25	14.81	16.10	17.84	17.34	16.69	na	15.63	16.59	16.48
Zr	118.0	104.5	143.5	132.2	119.4	123.9	113.8	123.2	117.0	na	100.0	101.7	131.7
Nb	3.64	4.90	7.40	5.38	3.01	3.35	3.46	3.65	3.35	na	3.08	3.02	4.30
Cs	0.51	0.63	0.61	0.54	0.63	0.64	0.53	0.66	0.57	na	0.52	0.52	0.77
Ba	525.9	543.2	537.9	455.3	534.5	506.5	471.2	539.2	456.0	na	472.5	485.3	604.0
La	11.36	8.73	14.32	9.96	13.83	13.36	13.02	13.52	11.30	na	11.29	11.13	11.35
Ce	25.57	18.74	31.04	21.57	30.13	29.42	29.13	29.66	23.23	na	25.07	24.79	24.37
Pr	3.33	2.39	3.78	2.66	3.46	3.36	3.44	3.44	2.92	na	2.94	2.96	3.08
Nd	14.63	10.35	14.91	10.90	15.23	15.10	15.82	15.60	12.56	na	13.40	13.90	13.08
Sm	3.29	2.46	3.54	2.78	3.37	3.43	3.66	3.48	3.10	na	3.16	3.32	2.88
Eu	1.07	0.84	1.09	0.93	1.01	1.06	1.17	1.10	1.01	na	1.00	1.06	0.96
Gd	3.01	2.44	3.12	2.73	3.04	3.07	3.47	3.17	3.02	na	2.95	3.22	2.73
Tb	0.48	0.40	0.51	0.47	0.45	0.47	0.52	0.49	0.49	na	0.47	0.49	0.43
Dy	2.93	2.50	2.77	2.68	2.69	2.80	3.10	3.00	2.97	na	2.86	3.05	2.68
Ho	0.62	0.52	0.53	0.53	0.52	0.56	0.62	0.60	0.62	na	0.57	0.60	0.57
Er	1.85	1.60	1.69	1.68	1.70	1.81	1.97	1.88	1.69	na	1.76	1.87	1.75
Tm	0.27	0.25	0.25	0.25	0.26	0.27	0.29	0.28	0.25	na	0.27	0.29	0.27
Yb	1.74	1.58	1.57	1.60	1.58	1.60	1.71	1.73	1.60	na	1.61	1.77	1.68
Lu	0.26	0.23	0.26	0.25	0.26	0.27	0.29	0.29	0.25	na	0.25	0.28	0.27
Hf	3.17	2.82	3.29	2.96	3.67	3.70	3.57	3.78	3.10	na	3.26	3.29	3.43
Ta	0.20	0.20	0.22	0.19	0.32	0.32	0.34	0.33	0.25	na	0.27	0.26	0.24
Tl	0.09	0.08	0.15	0.07	0.09	0.10	0.17	0.10	na	na	0.08	0.05	0.10
Pb	5.61	5.00	6.38	5.77	6.22	6.25	6.31	6.97	5.22	na	5.00	5.22	6.04
Th	1.66	1.55	1.89	1.52	2.13	2.25	1.99	2.23	1.64	na	1.86	1.77	2.00
U	0.73	0.64	0.69	0.57	0.74	0.76	0.64	0.72	0.60	na	0.62	0.68	0.82

TABLE 1. (continued)

	Basement	Xenoliths			Standards			
Sample	MZ-2	Xen-C	Xen-1810	Xen-B	BCU-3	BCU-3 CERT.	BIR-1	BIR-1 CERT
Location	Manzanillo	Cordobán	Cordobán	Cordobán				
Rock type	Granodiorite	Intermediate xenolith	Intermediate xenolith	Mafic xenolith	Basalt	Basalt	Basalt	Basalt
Mineralogy	Plg>FK>qz>hbl>bio	Plg>px>Gls	Plg>px>Gls>qz	Plg>px>Fe-Ti oxides>hbl				
Eruption date		unknown	unknown	unknown				
Latitude N	19°00′28″	19°29′19″	19°29′19″	19°29′19″				
Longitude W	104°14′37″	103°07′25″	103°07′25″	103°07′25″				
Major oxides (wt. %)								
SiO_2	63.93	61.73	65.09	46.18	50.79	50.58	47.64	47.77
TiO_2	0.89	0.35	0.38	3.23	1.78	1.75	0.97	0.96
Al_2O_3	14.84	19.54	18.51	16.33	16.03	16.17	15.55	15.35
Fe_2O_3 (t)	5.82	1.63	0.94	17.09	9.76	9.53	11.28	11.26
MnO	0.09	0.04	0.02	0.41	0.15	0.14	0.17	0.17
MgO	2.00	1.93	1.25	4.78	8.33	8.17	9.61	9.68
CaO	3.96	7.35	6.49	8.95	8.08	8.04	13.22	13.24
Na_2O	3.83	6.29	6.22	3.59	3.83	3.86	1.89	1.75
K_2O	4.04	0.51	0.79	0.33	1.11	1.15	0.04	0.03
P_2O_5	0.18	0.18	0.20	0.43	0.51	0.54	0.04	0.05
L.O.I.	0.22	0.30	0.32	–0.53				
SUM	99.81	99.85	100.21	100.81				
Trace elements (ppm)								
Ni	20.0	20.0	20.0	26.2			175	166
V	110.8	56.4	26.9	565.3			320	313
Cr	293.0	102.4	179.5	93.0			401	382
Co	12.5	2.7	1.0	33.8			51	51
Cu	29.0	13.8	33.2	349.6			126	126
Zn	89.2	30.0	30.0	327.0			69	71
Ga	19.1	20.6	20.2	25.4			16	16
Ge	1.83	1.57	1.48	2.63			1.50	1.50
Rb	148.3	2.9	5.8	3.9			<1	0.3
Sr	200.7	779.0	702.0	529.1			108	108
Y	36.06	11.91	13.34	39.90			16	16
Zr	466.4	176.4	139.0	160.8			16.0	15.5
Nb	11.58	3.74	3.39	5.08			0.50	0.60
Cs	3.81	0.10	0.11	0.11			<0.1	0.01
Ba	672.3	335.9	258.1	147.3			7.0	7.0
La	18.09	8.87	7.66	7.91			0.73	0.62
Ce	43.36	22.28	18.84	21.88			2.10	1.95
Pr	5.90	3.06	2.59	3.49			0.39	0.38
Nd	25.49	12.72	11.61	18.59			2.47	2.50
Sm	6.24	2.45	2.54	5.67			1.08	1.10
Eu	0.97	0.96	0.93	1.79			0.56	0.54
Gd	5.86	2.07	2.25	6.80			1.83	1.85
Tb	1.03	0.32	0.37	1.25			0.38	0.36
Dy	5.76	1.80	2.03	7.23			2.69	2.50
Ho	1.15	0.37	0.42	1.46			0.59	0.57
Er	3.63	1.17	1.32	4.39			1.78	1.70
Tm	0.57	0.18	0.21	0.65			0.28	0.26
Yb	3.50	1.23	1.33	3.77			1.66	1.65
Lu	0.54	0.21	0.23	0.56			0.25	0.26
Hf	10.82	3.49	3.15	3.87			0.60	0.60
Ta	0.91	0.16	0.24	0.34			0.02	0.04
Tl	0.47	0.08	0.05	0.05			<0.05	0.01
Pb	8.87	5.00	5.00	5.00			<5	3.00
Th	10.20	1.01	1.17	0.54			<0.02	0.03
U	3.69	0.39	0.15	0.22			0.01	0.01

Notes: *—data performed by Activation Laboratories; **—data provided by J. Luhr (personal commun.) based on XRF (Smithsonian Institution) and ICP-MS (Washington State University) Samples without asterisks were analyzed at LUGIS, Instituto de Geología, UNAM. BCU-3—internal laboratory standard (LUGIS); BIR-1—standard used by Activation Laboratories; L.O.I.—loss on ignition; CERT—certified values; na—not analyzed.

TABLE 2. MODAL ANALYSES (VOL%) FOR COLIMA VOLCANO SAMPLES OBTAINED FROM POINT-COUNTING (800 POINTS) OF REPRESENTATIVE THIN SECTIONS

Eruption date:	1869	1962	1913	1998	2001	2002	1818	1913	Prehistorical
Rock type:	Andesite	Andesite	Andesite	Andesite	Andesite	Andesite	Andesite	Andesite	Andesite
Sample ID:	Col-1	Col-2	Col-3	Col-4	Col-5	Col-6	Col-9	Col-12	Col-14B
Eruptive products:	lava	lava	pumice	lava	dome	dome	pumice	scoria	dome
Phn-Plagioclase	20.8	36.1	12.6	26.3	29.3	21.8	15.6	11.1	20.1
Mph-Plagioclase	3.9	5.4	2.3	1.5	2.9	4.0	3.1	4.3	8.4
Phn-Hypersthene	1.0	2.0	1.4	3.4	5.0	5.0	3.0	4.5	1.4
Mph-Hypersthene	1.3	2.6	1.5	2.0	2.1	3.0	3.5	0.9	2.9
Phn-Augite	0.4	1.5	2.8	1.6	3.5	2.6	0.1	2.0	0.0
Mph-Augite	0.5	1.3	1.6	1.0	0.9	1.5	0.4	0.0	1.4
Phn-Hornblende	1.8	0.0	2.6	1.0	0.0	0.1	0.0	0.1	6.3
Mph-Hornblende	0.0	0.0	0.6	0.0	0.0	0.0	0.0	0.1	0.3
Fe-Ti oxides	1.6	1.4	0.5	0.8	0.9	1.3	0.3	1.0	1.6
Phn-Olivine	0.0	0.0	0.1	0.0	0.0	0.0	0.0	0.0	0.0
Mph-Olivine	0.0	0.0	0.0	0.1	0.0	0.0	0.1	0.0	0.0
Crystals	31.1	50.3	26.0	37.6	44.5	39.3	26.1	24.0	42.3
Groundmass	68.9	49.8	74.0	62.4	55.5	60.8	73.9	76.0	57.8

Note: Phn—Phenocryst > 0.3 mm. Mph—Microphenocryst < 0.3 mm (after Wilcox, 1954).

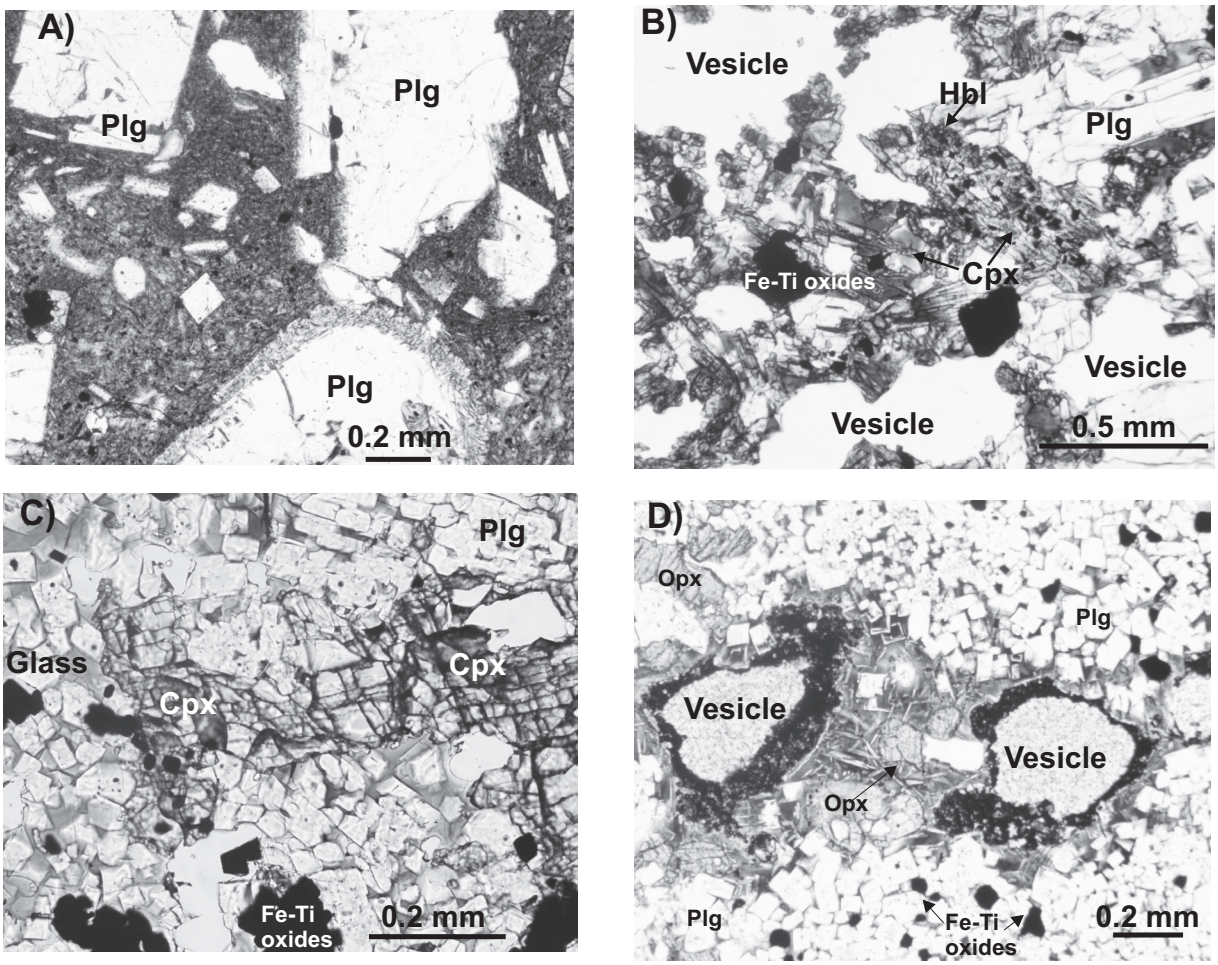

Figure 4. Photomicrographs in transmitted plane light. (A) Prehistorical lava flow (Col-20). The glass-rich groundmass zone encloses the lower plagioclase crystal, which has corroded rims, while plagioclase (Plg) above is unaffected. (B) Xenolith hosted in Col-20 lava flow, with quenched textures evidenced by acicular crystals of randomly oriented pyroxene set in brown glass. (C) Mafic xenolith (Xen-B) showing pyroxene crystals corroded by brown glass and abundant Fe-Ti oxides. Equidimensional plagioclase crystals form aggregates in brown glass. (D) Xenolith hosted in the 1998 lava flow (Col-4) showing corroded pyroxene crystals in the upper left part and rounded crystals in the central part. Note the acicular plagioclase crystals in interstitial brown glass and the stout prismatic plagioclase with less-abundant interstitial glass in the central part of the section. Xenoliths shown in B and D were only analyzed petrographically. Plg—plagioclase; Hbl—hornblende; Cpx—clinopyroxene; Opx—orthopyroxene.

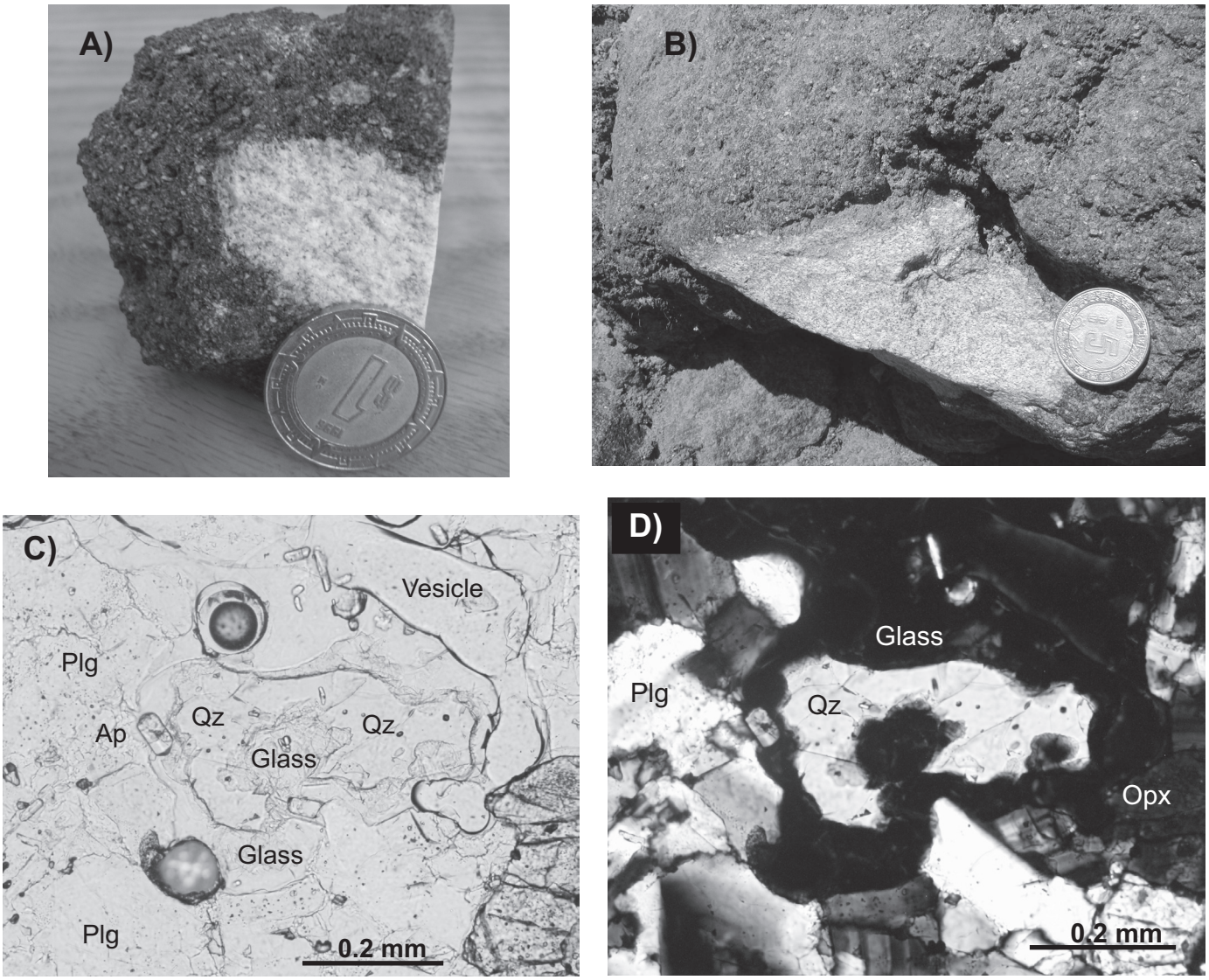

Figure 5. Granodioritic xenoliths: (A) Hand specimen of a granodioritic pink-green xenolith (Xen-1810) with rounded borders, hosted in a prehistorical andesite talus block. The coin diameter is 2 cm. (B) Hand specimen of a granodioritic xenolith (Xen-C) hosted in a prehistorical lava flow near the 1998 lava flow front. Coin size is ~3 cm. (C) Photomicrograph of xenolith Xen-1810 in transmitted plane-polarized light showing corroded quartz (Qz) with glass embayments, dusty plagioclase (Plg) near the left border of the microphotograph, and apatite (Ap) crystals in the center. (D) Same field as C in transmitted cross-polarized light; Opx—orthopyroxene.

were determined by fusion inductively coupled plasma–emission spectrometry (ICP-ES) at Activation Laboratories in Canada. Trace-element concentrations of all samples were determined by fusion inductively coupled plasma–mass spectrometry (ICP-MS) at the same laboratory.

Isotope ratios of $^{87}Sr/^{86}Sr$, $^{143}Nd/^{144}Nd$, $^{206}Pb/^{204}Pb$, $^{207}Pb/^{204}Pb$, and $^{208}Pb/^{204}Pb$ were determined in 15 selected samples from Colima volcano (Pb isotopes were measured from only 11 samples). Powdered whole-rock aliquots (150 mg) were leached in Teflon bombs with 6*N* HCl for 2 h at a constant temperature of 90 °C to remove possible ambient Pb and then dissolved in a HF-HNO_3 (3:1) mixture. Pb was separated using small Teflon tube columns filled with DOWEX anion-exchange resin. Sr and rare earth elements (REEs) were separated using quartz-glass columns filled with DOWEX cation-exchange resin. Nd was further separated using small quartz columns filled with Teflon powder coated with hydrogen diethylhexyl-phosphate (HDEHP). All samples were analyzed on a Finnigan MAT-262 thermal-ionization mass spectrometer, equipped with a variable multicollector system (8 Faraday cups) in static mode at LUGIS, Instituto de Geofísica, UNAM. Results were corrected for mass fractionation by normalizing to $^{87}Sr/^{86}Sr = 0.1194$ and $^{143}Nd/^{144}Nd = 0.7219$.

The fractionation factor for Pb isotope ratios was determined by comparison with the mean value of the Pb NBS 981 standard (see Table 3).

Oxygen isotopes were performed with a stable isotope mass spectrometer SIRA12 (Micromass, UK) coupled with a CO_2 laser-BrF_5 fluorination technique at the Institute for Study of the Earth's Interior (ISEI), Okayama University at Misasa, Japan (Kusakabe et al., 2004). All $\delta^{18}O$ values were referenced to the Vienna standard mean ocean water–standard light Antarctic precipitation (V-SMOW-SLAP) scale. We obtained $\delta^{18}O$ values of 9.30‰, 5.01‰, and 5.72‰ for NBS-28 quartz, NBS-30 biotite, and UWG2 garnet standards, respectively. All isotopic results are presented in Table 3.

MAJOR- AND TRACE-ELEMENT GEOCHEMISTRY

Major- and trace-element concentrations are given in Table 1. Prehistorical lavas show whole-rock silica contents from 58.05 to 60.6 wt%. Lava flow Col-19 shows the lowest SiO_2 concentration, whereas the highest value is observed in the Los Hijos del Volcán dome sample Col-14B. MgO ranges from 3.4 to 4.2 wt%, with sample Col-19 displaying the highest content. SiO_2 in historical lavas varies from 58.2 to 61.4 wt%, and MgO contents are between 2.8 and 4.5 wt%, with the highest value corresponding to scoria sample Col-12. Both prehistorical and historical lavas are andesitic in composition.

The mafic xenolith (Xen-B) has 46.2 wt% SiO_2 and 4.8 wt% MgO, whereas the intermediate to felsic xenoliths (Xen-C and Xen-1810) have 61.7 and 65.1 wt% SiO_2, and 1.93 and 1.25 wt% MgO, respectively. Xen-B has a gabbroic composition, whereas Xen-1810 and Xen-C have granodioritic compositions.

Different major and trace elements are plotted versus SiO_2 in Figure 6. In both prehistorical and historical lavas, MgO, TiO_2, Ni, V, Co, and Cr (Fig. 6A–B) show negative correlations with SiO_2, suggesting fractional crystallization of olivine, titanomagnetite, and pyroxene. Na_2O and Al_2O_3 show inconsistent trends versus SiO_2, probably as a result of plagioclase fractionation or accumulation (Fig. 6A). On the other hand, CaO shows a well-defined negative correlation with increasing SiO_2, probably due to the fractionation of pyroxene (Fig. 6A). P_2O_5 displays considerable scatter (not shown in Fig. 6), but a positive correlation with SiO_2 can be observed in the historical lavas. This positive correlation can be best explained by fractional crystallization of apatite, a mineral that was observed as an accessory phase in thin sections. In all Harker-type diagrams of Figure 6, the three xenoliths and the Manzanillo granodiorite are plotted for comparison.

In a multi-element diagram for prehistorical and historical lavas (Fig. 7), enrichments in large ion lithophile elements (LILEs) with respect to high field strength elements (HFSEs) are evident. Negative anomalies of Nb and Ti are present in all suites, indicating a typical subduction signature. Positive anomalies for Pb and Ba suggest contributions from subducted sediments, whereas those for K and Zr are possibly caused by the assimilation of basement rocks from the Manzanillo Batholith. Xenoliths show depletions in LILEs (e.g., Cs, Rb, Ba, K) compared with the lavas.

Prehistorical and historical lavas display enrichments of light rare earth elements (LREEs) with a flat heavy rare earth

TABLE 3. STRONTIUM, NEODYMIUM, LEAD, AND OXYGEN ISOTOPE RATIOS OF PREHISTORICAL AND HISTORICAL SAMPLES FROM COLIMA VOLCANO

Sample	Eruptive event	$^{87}Sr/^{86}Sr$	$\pm1\sigma_{abs}$	$^{143}Nd/^{144}Nd$	$\pm1\sigma_{abs}$	ε_{Nd}	$^{206}Pb/^{204}Pb$	$\pm1\sigma_{rel}$	$^{207}Pb/^{204}Pb$	$\pm1\sigma_{rel}$	$^{208}Pb/^{204}Pb$	$\pm1\sigma_{rel.}$	$\delta^{18}O$ (‰)	σ
Col-1	1869	0.703565	37	0.512961	20	6.30	18.571	0.062	15.562	0.069	38.288	0.087	5.81	0.07
Col-2	1962	0.703569	32	0.512964	19	6.36	18.577	0.049	15.570	0.055	38.315	0.065	5.69	0.11
Col-3	1913	0.703542	37	0.512975	21	6.57	18.585	0.035	15.587	0.041	38.361	0.048	5.68	0.00
Col-4	1998	0.703605	38	0.512931	23	5.72	18.571	0.030	15.564	0.030	38.285	0.032	5.81	0.13
Col-4R	1998	0.703561	41	0.512916	18	5.42	18.568	0.057	15.556	0.064	38.260	0.061	na	na
Col-5	2001	0.703551	39	0.512929	24	5.68	18.573	0.031	15.568	0.032	38.298	0.034	6.09	0.10
Col-5R	2001	0.703595	36	na	na	na	18.560	0.067	15.548	0.064	38.238	0.066	na	na
Col-6	2002	0.703564	40	0.512993	16	6.92	18.570	0.035	15.563	0.040	38.285	0.048	5.80	0.35
Col-9	1818	0.703535	39	0.512911	20	5.33	18.587	0.047	15.573	0.050	38.323	0.053	6.38	0.02
Col-12	1913	0.703570	38	0.512922	15	5.54	18.610	0.075	15.598	0.089	38.410	0.111	na	na
Col-14B	Prehistorical	0.703614	39	0.512927	18	5.64	18.583	0.042	15.571	0.040	38.320	0.042	6.16	na
Col-18	1975	0.703555	39	0.512947	16	6.03	18.586	0.037	15.580	0.039	38.346	0.038	6.84	0.10
Col-19	Prehistorical	0.703551	39	0.512936	25	5.81	18.567	0.059	15.565	0.061	38.288	0.063	na	na
Col-20	Prehistorical	0.703581	39	0.512919	18	5.48	na		na		na		6.85	0.10
XENC		0.703874	39	0.512877	15	4.66	na		na		na		7.08	na
XEN1810		0.703937	40	0.512936	16	5.81	na		na		na		6.84	0.10
XENB		0.703931	38	0.512938	23	5.85	na		na		na		6.43	0.18

Notes: $1\sigma_{abs.}$ error refers to the last two digits. Laboratory values of NBS 987 Sr standard, the Nd La Jolla standard, and the NBS 981 Pb standard are: $^{87}Sr/^{86}Sr = 0.710235 \pm 18$ ($1\sigma_{abs.}$; n = 275); $^{143}Nd/^{144}$ Nd = 0.511877 ± 21 ($1\sigma_{abs.}$; n = 140); $^{206}Pb/^{204}Pb = 16.8926 \pm 0.04\%$ ($1\sigma_{rel.}$), $^{207}Pb/^{204}Pb = 15.4272 \pm 0.06\%$, $^{208}Pb/^{204}Pb = 36.5090 \pm 0.08\%$ (n = 80). Total blanks during the run of these samples were 3.6 ng for Sr, 0.17 ng for Nd, and 233 pg for Pb. Samples were loaded as chlorides on double rhenium filaments (Sr and Nd) or as silica gel-H_3PO_4 mixtures on single rhenium filaments (Pb). Sixty isotope ratios were determined for Sr and Nd, and one hundred runs were performed for Pb. Data were not further corrected. Oxygen data were analyzed two to four times, except samples Col-14B and Xen-C. Mean values and standard deviations are given. Na—not analyzed; R—replicate analysis.

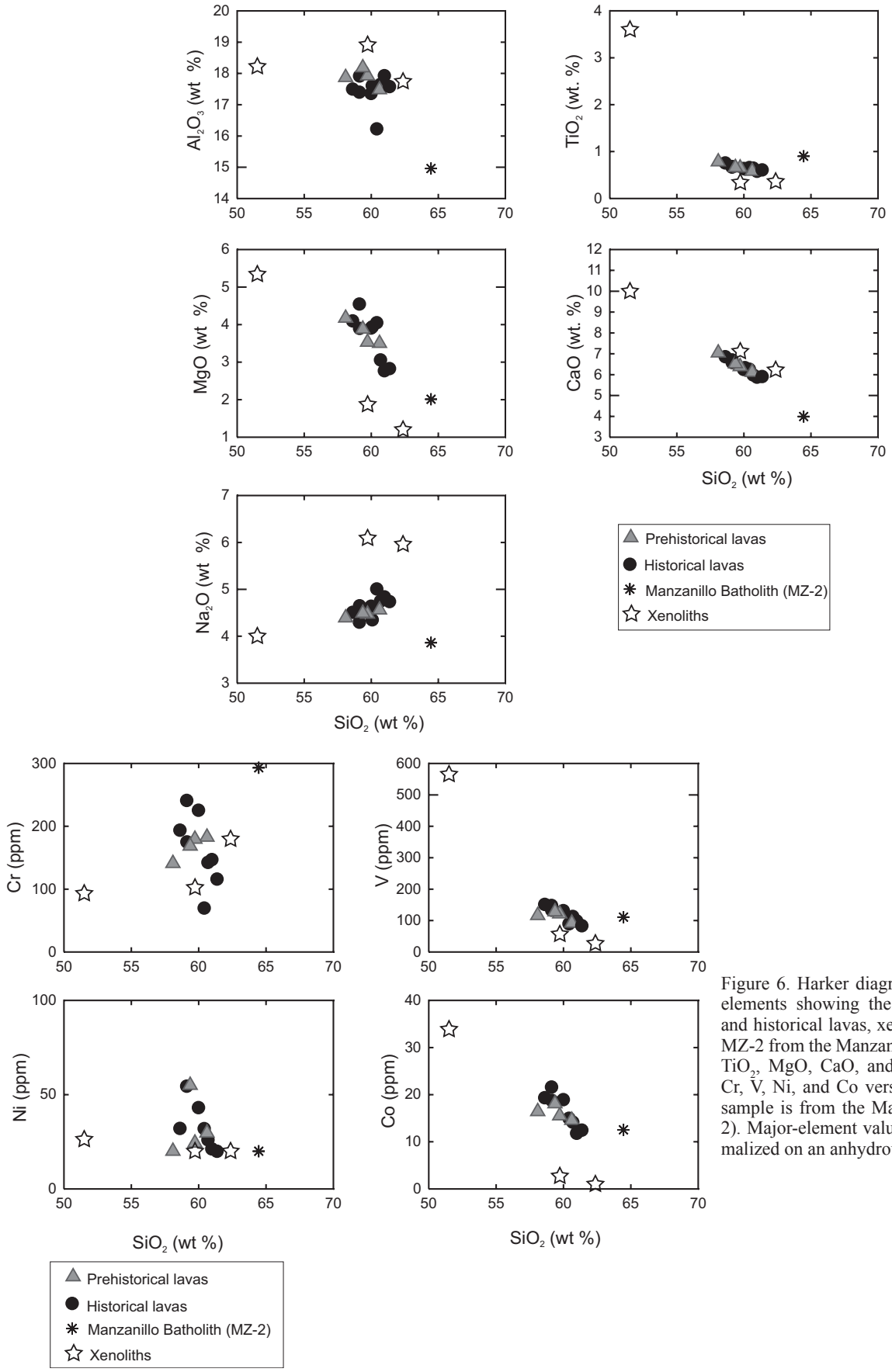

Figure 6. Harker diagrams for major and trace elements showing the trends for prehistorical and historical lavas, xenoliths, and granodiorite MZ-2 from the Manzanillo Batholith. (A) Al_2O_3, TiO_2, MgO, CaO, and Na_2O versus SiO_2; (B) Cr, V, Ni, and Co versus SiO_2. Basement rock sample is from the Manzanillo Batholith (MZ-2). Major-element values from Table 1 are normalized on an anhydrous basis.

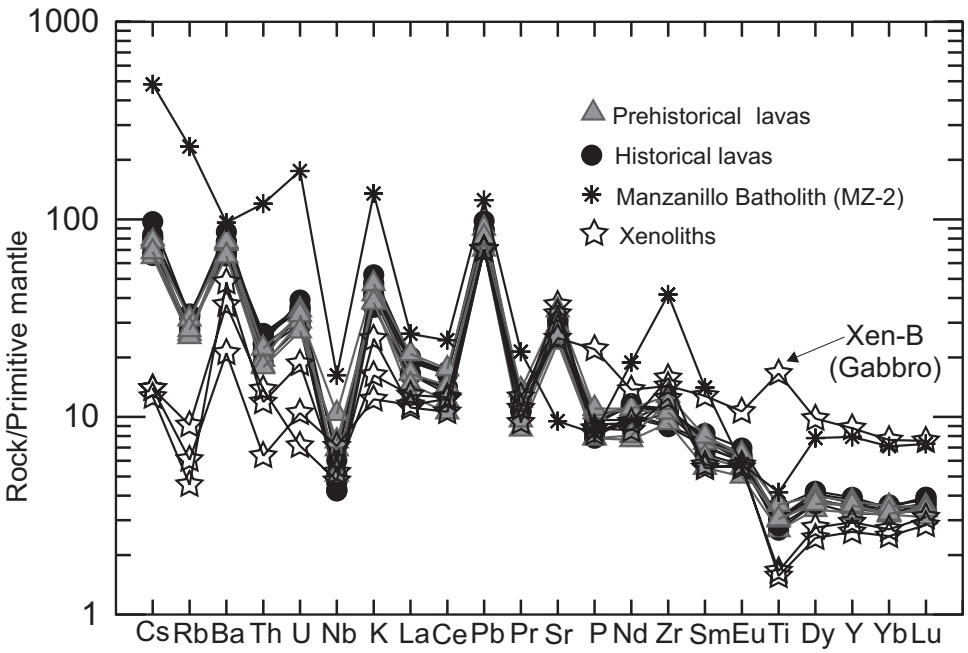

Figure 7. Primitive mantle–normalized (Sun and McDonough, 1989) multi-elemental diagram for prehistorical and historical lavas, xenoliths, and granodiorite MZ-2 from the Manzanillo Batholith.

element (HREE) pattern (Fig. 8). This nearly horizontal distribution of the HREE and low La/Yb ratios (<10) are consistent with the absence of garnet in the source rock. Low values of Sm/Yb (<3) are compatible with a low-pressure, pyroxene-dominated residual mineral assemblage, as observed by Kay et al. (1999) in the southern Central volcanic zone of the Andean arc, where the crustal thickness (30–35 km) is comparable to the area beneath Colima volcano. Xenoliths (Xen-C and Xen-1810) show similar LREE patterns, but significant depletion of the HREE with respect to the historical and prehistorical lavas (Fig. 8). Xen-B also shows subhorizontal REE behavior, but interestingly, a HREE pattern nearly identical to the Manzanillo granodiorite (MZ-2). Both samples are significantly enriched in HREE with respect to the Colima volcano lavas.

SR-ND-PB-O ISOTOPE DATA

Sr, Nd, and Pb isotope ratios are listed in Table 3 and are plotted in Figure 9 ($^{87}Sr/^{86}Sr$ vs. ε_{Nd}) and Figure 10 ($^{206}Pb/^{204}Pb$ vs. $^{207}Pb/^{204}Pb$ and $^{206}Pb/^{204}Pb$ vs. $^{208}Pb/^{204}Pb$). The isotopic com-

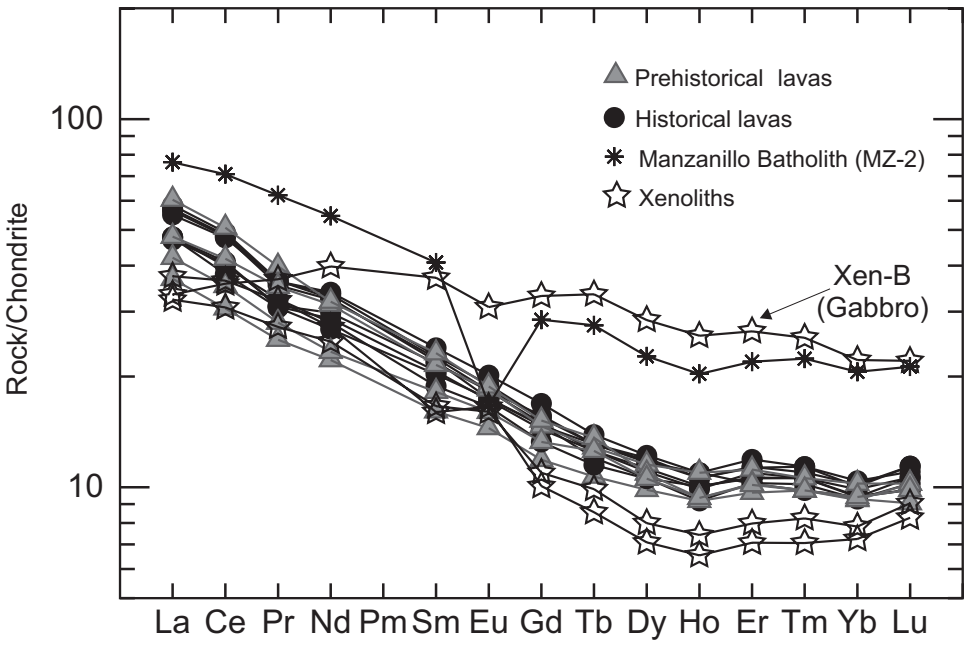

Figure 8. Chondrite-normalized (Sun and McDonough, 1989) rare earth element diagram showing patterns for prehistorical and historical lavas, xenoliths, and granodiorite from the Manzanillo Batholith.

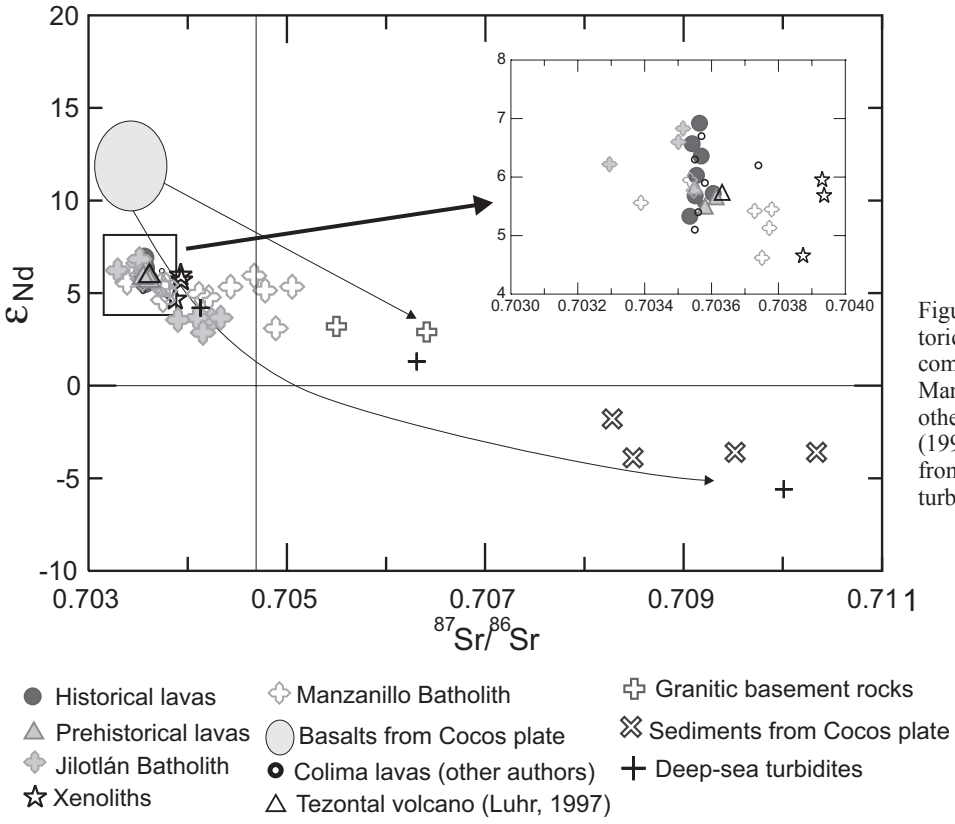

Figure 9. $^{87}Sr/^{86}Sr$ versus ε_{Nd} diagram for prehistorical and historical Colima volcano samples compared with data from Schaaf (1990) for the Manzanillo and Jilotlán Batholiths. Data for other granitic basement rocks are from Luhr (1997), for Cocos plate basalts and sediments from Verma (2000), and for Pacific deep-sea turbidites from McLennan et al. (1990).

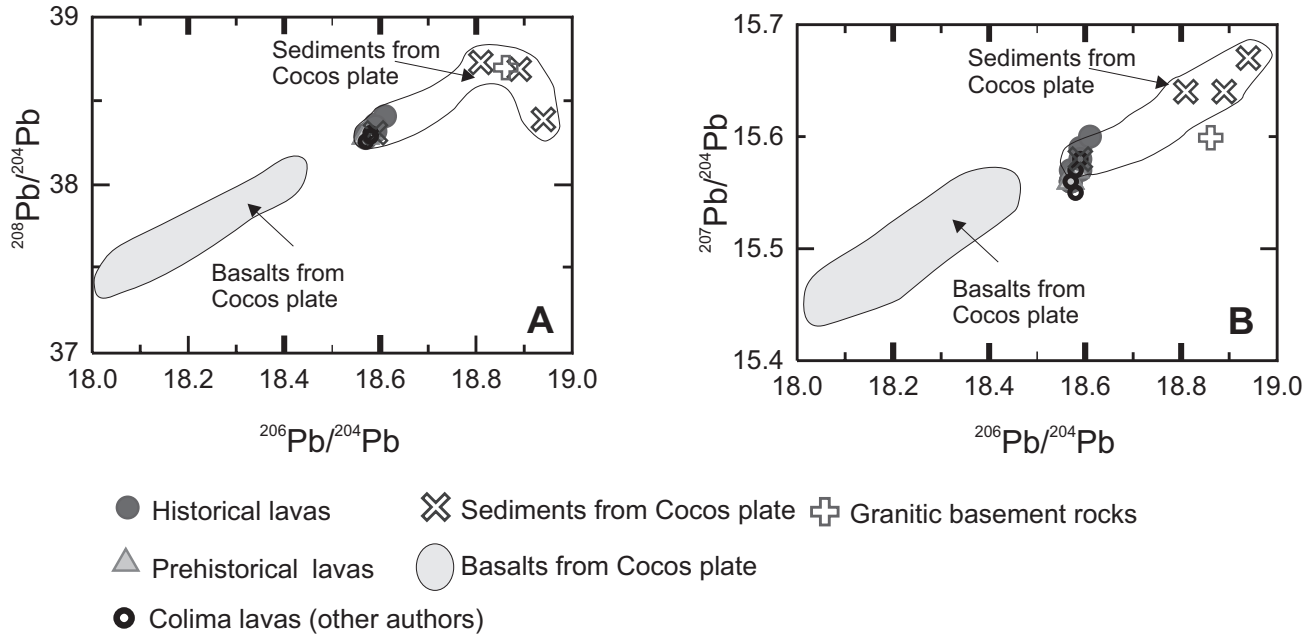

Figure 10. Pb isotopic variation diagram for Colima volcano samples. (A) $^{208}Pb/^{204}Pb$ versus $^{206}Pb/^{204}Pb$, (B) $^{207}Pb/^{204}Pb$ versus $^{206}Pb/^{204}Pb$. Data sources for granitic basement rocks, basalts, and sediments are as in Figure 9.

position of the prehistorical Colima lavas is $^{87}Sr/^{86}Sr$: 0.70355–0.70361, ε_{Nd}: +5.5 to +5.8, $^{206}Pb/^{204}Pb$: 18.57–18.58, $^{207}Pb/^{204}Pb$: 15.56–15.57, and $^{208}Pb/^{204}Pb$: 38.29–38.32. Historical Colima volcano products display $^{87}Sr/^{86}Sr$ from 0.70354 to 0.70361, ε_{Nd} from +5.3 to +6.9, $^{206}Pb/^{204}Pb$ from 18.57 to 18.61, $^{207}Pb/^{204}Pb$ from 15.56 to 15.60, and $^{208}Pb/^{204}Pb$ from 38.28 to 38.41. The most recent product (2002 dome sample Col-6) shows the highest ε_{Nd} and lowest $^{206}Pb/^{204}Pb$ and $^{207}Pb/^{204}Pb$ values. For all samples, $^{87}Sr/^{86}Sr$ shows a very small variation with time. Previously published isotope data (Moorbath et al., 1978; Verma and Luhr, 1993; Luhr, 1997; Lassiter and Luhr, 2001) are very similar to our new data.

Colima volcano isotope data are compared in Figure 9 with data from the Manzanillo and Jilotlán Batholiths (Schaaf, 1990) and data from deep-sea turbidites from the Middle America Trench (McLennan et al., 1990). Additionally, Sr, Nd, and Pb isotope data from Colima volcano published by Luhr (1997) and from Cocos plate basalts and sediments (Verma, 2000) are shown in Figures 9 and 10. Colima lavas have nearly identical ε_{Nd} parameters to the Manzanillo and Jilotlán plutonic rocks and plot within the $^{87}Sr/^{86}Sr$ data field of these Mesozoic intrusives. Colima volcano isotope data can be interpreted as a three-component mixture of basalts, deep-sea sediments, and turbidites, as deduced from their intermediate position in Figure 9 with respect to these sources.

$^{18}O/^{16}O$ ratios were obtained from 10 andesitic whole-rock samples and three xenoliths hosted in prehistorical lava flows (Table 3). Prehistorical lavas have $\delta^{18}O$ values ranging from +6.2‰ to +6.8‰, whereas historical lava flows show slightly lower $\delta^{18}O$, between +5.7‰ and +6.4‰. Xenoliths display $\delta^{18}O$ from +6.4‰ to +7.1‰. Oxygen isotope data for Colima volcano lavas are similar and typical of andesites erupted in island arcs and active continental margin regimes around the Pacific Ocean (McBirney et al., 1987). The $\delta^{18}O$ isotope data are plotted versus $^{87}Sr/^{86}Sr$ ratios in Figure 11A and versus ε_{Nd} in Figure 11B, which also includes data from Paricutín volcano (McBirney et al., 1987), Manzanillo and Jilotlán Batholiths, and basalts east of Tecalitlán, Jalisco (Schaaf, 1990).

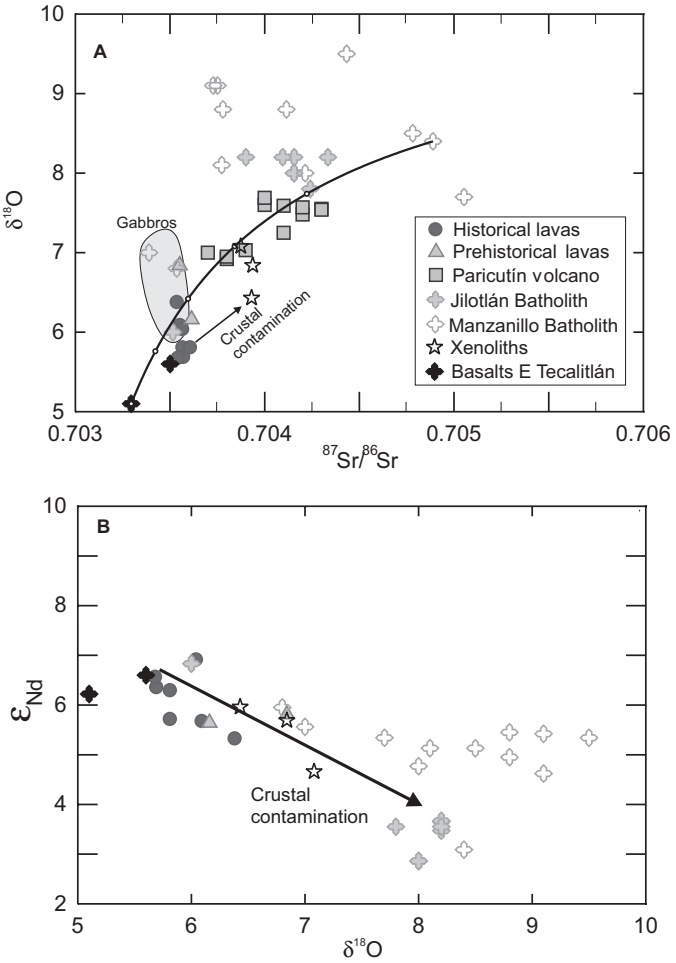

Figure 11. (A) $^{87}Sr/^{86}Sr$ versus $\delta^{18}O$ diagram for Colima volcano products. Data source for Paricutín volcano: McBirney et al. (1987); and for Manzanillo and Jilotlán Batholiths, including two basalt samples from the western border of the Jilotlán Batholith (east of Tecalitlán): Schaaf (1990). Mixing line (black) is between one of the most radiogenic $^{87}Sr/^{86}Sr$ of the Manzanillo Batholith samples and the less radiogenic basalt east of Tecalitlán. (B) $\delta^{18}O$ versus ε_{Nd} diagram showing the effects of crustal contamination indicated by an arrow pointing toward the Manzanillo and Jilotlán Batholiths.

DISCUSSION

Colima volcano is located at the western front of the Mexican volcanic belt, only 150 km NE of the Middle America Trench, where subduction of the Rivera-Cocos plate boundary has been taking place beneath the North American plate (Fig. 1). This boundary is oriented N40E, extending from the El Gordo graben (Fig. 1) to at least 19.3°N to 103°W as proposed by Bandy et al. (1995). These authors concluded that divergence along the boundary induces thermal convection, which heats the overlying mantle, causing uplift, thinning, and stretching of the overlying crust. They also proposed that the mantle-crust boundary is located at a depth between 28 and 35 km. The geometry of the subducted Cocos plate was discussed by Pardo and Suárez (1995), emphasizing a dip of ~50° of the subducting slab and an overall depth of 100 km for the subducted plate beneath Colima volcano.

With this tectonic framework in mind, the following discussion will address different aspects of magma generation at Colima volcano, such as the influence of the subducting slab, magma mixing, fractional crystallization, and crustal contamination.

Signals of the Subducting Slab

Subduction signatures in relatively evolved magmas such as the Colima volcano andesites are difficult to discern, since differentiation and crustal contamination processes disguise elemental and isotope ratios. However, lavas from Colima volcano show positive peaks in Pb, Ba, K, and Sr in multi-element

diagrams, normalized to primitive mantle values (Fig. 7), suggesting involvement of sediment-derived fluxes from the subducting slab.

As a consequence of the oblique subduction of the Cocos and Rivera plates beneath the North America plate, in the Colima area (western Mexican volcanic belt; Fig. 1) relatively young and hot oceanic lithosphere is being subducted. In contrast, beneath the central and eastern Mexican volcanic belt, the subducting slab is composed of older and cooler material. These effects can contribute to different amounts of volatile elements, such as Cs and Rb, along the Mexican volcanic belt, corresponding to different thermal structures of the slab, as proposed by Gómez-Tuena et al. (2004). For the case of Colima volcano samples, we observe slightly lower Cs and Rb values (60–100 times primitive mantle values; Fig. 7) in comparison to central Mexican volcanic belt Popocatépetl lavas (110–120 times primitive mantle values; Schaaf et al., 2005), which can confirm the arguments of these authors emphasizing the importance of slab-derived fluids in magma generation, but can also be explained by different mixtures of a heterogeneous upper mantle and different lithologies in the continental crust.

Regarding the isotope data displayed in $^{87}Sr/^{86}Sr$ versus ε_{Nd} and $^{206}Pb/^{204}Pb$ versus $^{207}Pb/^{204}Pb$ and $^{208}Pb/^{204}Pb$ diagrams (Figs. 9 and 10, respectively), Colima volcano samples are placed in an intermediate position between mid-ocean-ridge basalts (MORB) and Cocos plate sediments, signifying both as possible source materials in parental melt generation.

Magma Mixing

Magma mixing was probably an important process during Colima volcano evolution and was discussed in detail by Luhr and Carmichael (1980), Robin et al. (1991), and Mora et al. (2002). During the 1818–1913 events, Robin et al. (1991) proposed a mixing stage between a differentiated magmatic body and a new "mafic input." They suggested that the long effusive/extrusive phases correspond to the ensuing differentiation stage of the new magmatic body. Luhr and Carmichael (1980) discussed magma mixing processes as a result of anomalous enrichments of compatible trace elements in the hornblende and olivine andesites from Colima volcano. They also focused on textural evidence for mixing in andesites, like the presence of glass inclusion–riddled plagioclase cores surrounded by sodic, inclusion-free rims, and reverse zoning of orthopyroxene and clinopyroxene. Mora et al. (2002) proposed mixing between two andesitic magmas with different silica contents, degrees of evolution, and crystal contents.

We observed olivine xenocrysts (e.g., in the 1913 fall deposits) frequently mantled by reaction rims composed of symplectitic titanomagnetite, pyroxene, and plagioclase, suggesting disequilibrium with the andesitic matrix and a mafic origin for such xenocrysts. However, the striking isotopic homogeneity of the Colima volcano andesites doesn't allow the identification of individual mixing components. On the other hand, olivine xenocrysts are relatively rare (~0.1%, Table 2) in comparison to other Mexican volcanic belt stratovolcanoes (e.g., Iztaccíhuatl [Nixon, 1988]; Popocatépetl [Schaaf et al., 2005]), and together with the homogeneous Sr-Nd-Pb isotope ratios, we suggest that mixing processes are not dominant in the evolution of Colima volcano magmas.

Fractional Crystallization

Fractional crystallization played an important role during the differentiation of the Colima volcano andesites. Evidence is given by the petrography of the lavas (e.g., the presence of plagioclase and pyroxene phenocrysts) and some elemental trends (e.g., high content of Fe-Ti oxides) as discussed herein. Sr isotope data also emphasize the importance of fractional crystallization during magma genesis regarding the horizontal and very homogeneous distribution of $^{87}Sr/^{86}Sr$ ratios in a 1/Sr versus $^{87}Sr/^{86}Sr$ diagram, which is not shown here.

The discussion of whether Colima volcano magmas fractionated in a closed or open system can be partly resolved when looking at oxygen isotope variations. Taylor and Sheppard (1986) showed that in a closed fractional crystallization system, the $\delta^{18}O$ of the final melt can never deviate appreciably from the initial $\delta^{18}O$ of the melt. In this case, only slight increments (<0.2–0.8‰) during differentiation are observed. The authors concluded that as a general principle, variations larger than 1‰ would necessarily imply other processes in addition to crystal fractionation, which is the case of Colima volcano magmas, displaying $\delta^{18}O$ variations up to 1.17‰ (Table 3).

Our Colima volcano samples do not show a systematic correlation between $^{87}Sr/^{86}Sr$ ratios and SiO_2. Calc-alkaline basalts from surrounding areas, such as Tezontal volcano southeast of Ciudad Guzmán (Luhr, 1997) and to the east of Tecalitlán, Jalisco (Fig. 3) (Schaaf, 1990), which can be considered as primitive parental magmas for Colima volcano, show $^{87}Sr/^{86}Sr$ ratios identical to those of Colima volcano andesites (Fig. 12).

This points to Assimilation and Fractional Crystallization (AFC) processes that involve assimilants having little isotopic contrast with the magma, which makes the distinction between upper- and lower-crustal contributions ambiguous. In the case of the Colima volcano magmas, the physical evidence for crustal contamination is strongly supported by the presence of partially melted granitoid xenoliths. For this reason we address our attention to crustal contamination as an important open-system process involved in the genesis of the Colima volcano magmas.

Crustal Contamination

Considering that the crust beneath Colima volcano is between 28 and 35 km thick, and using the existing geological information for this crust, (granodioritic basement, ca. 69 Ma; Allan, 1986; Schaaf, 1990), we discuss the role of crustal contamination during the generation of Colima volcano andesites, based on field observations, petrography, and geochemical evidence.

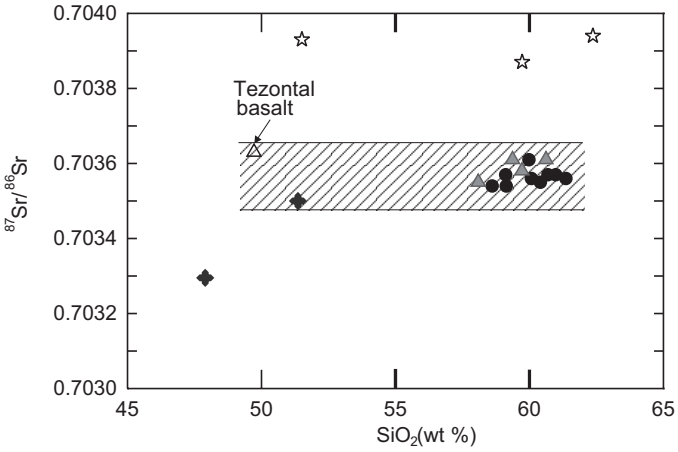

Figure 12. SiO_2 versus $^{87}Sr/^{86}Sr$ diagram for Colima volcano lavas. Dashed area includes basalts from Tezontal volcano (Luhr, 1997) and east of Tecalitlán (Schaaf, 1990), considered to represent primitive parental Colima volcano magmas. Symbols are as in Figure 11.

The presence of mafic and intermediate vesicular intrusive xenoliths hosted in some prehistorical andesitic magmas (like sample Col-20) offers evidence of magma-crust interaction during magma evolution. Similar plutonic clasts were found in the 2001 pyroclastic flow deposit. Petrographic evidence of partial melting in these xenoliths is shown in Figures 5C and 5D, and includes of the presence of brown to colorless glass, melted quartz, corroded pyroxene partly replaced by glass, and plagioclase recrystallization. The presence of glass suggests that the liquid formed at the xenolith rims was quenched (Cox et al., 1979). During the ascent of the andesitic magma, short tabular plagioclase crystals formed, as signified by pockets of crystals in brown glass (Fig. 4C–D), suggesting that these xenoliths were engulfed by andesitic magma at a temperature above the xenolith solidus temperature.

Based on existing work and on our new geochemical data for Colima volcano, we propose that partial melting of the mantle wedge for Colima magmas occurred in a garnet-free zone, where a first accumulation of primitive magma was stored. The most significant evidence for this is the inherited REE distribution from the garnet-free source. During magma ascent, the already differentiated magma was stored in a shallow-level reservoir, hosted in an intrusive complex beneath Colima volcano. As shown by the xenolith samples (Xen-C, Xen-1810), blocks of plutonic host rocks were dropped into the magma chamber and were incompletely assimilated (Fig. 5A–B). If the residence time of these xenoliths in the magma chamber had been sufficiently long, assimilation processes would have occurred. In the case of Colima volcano, we suggest that the plutonic basement is formed by the Manzanillo and Jilotlán Batholiths (Fig. 3). Following this idea, Colima volcano magmas underwent intense fractional crystallization and were "contaminated" with a plutonic basement with similar isotopic signatures ($^{87}Sr/^{86}Sr$: 0.7035–0.7048; ε_{Nd}: +3.1 to +7). For this reason, no major isotopic differences between the Colima volcano magmas and the contaminant crust are identifiable. It is worth mentioning that isotopically, the Manzanillo and Jilotlán Batholiths represent the most primitive plutonic rocks of the Mexican Cordillera (Schaaf, 1990).

Our interpretations are generally in accordance with those of Lassiter and Luhr (2001), who proposed on the basis of Os isotope data that only small quantities of lower-crustal assimilation is required to produce the observed isotopic range in the Mexican volcanic belt samples. They also emphasized that such contamination would produce only minor changes in the Sr, Nd, and Pb isotopic compositions of the magmas.

In contrast to the Sr and Nd isotopic systems, oxygen isotopes differ substantially if we compare the Colima volcano andesites with the Manzanillo and Jilotlán intrusives (Fig. 11A). Only three gabbros from both complexes plot within or near the Colima volcano field ($\delta^{18}O$ from +6.0‰ to +7.0‰). The other gabbros, tonalites, and granodiorites have significantly higher $\delta^{18}O$ values (+7.7‰ to +9.1‰; values from Schaaf [1990]). For comparison, we have also plotted in Figure 11A the $^{87}Sr/^{86}Sr$ ratios and $\delta^{18}O$ values for two samples of basaltic composition found east of Tecalitlán (Fig. 3). These samples can be regarded as representative of a nearly undifferentiated, primitive upper mantle and have lower $\delta^{18}O$ and $^{87}Sr/^{86}Sr$ than the Colima volcano samples. Colima volcano andesites are situated on a mixing line between basaltic and plutonic end members in Figure 11A. The Colima volcano data do not show a correlation between $^{87}Sr/^{86}Sr$ and $\delta^{18}O$, as would be expected for the case of crustal contamination with the Manzanillo and Jilotlán Batholiths (Fig. 11A), but rather they show constant $^{87}Sr/^{86}Sr$ ratios with respect to $\delta^{18}O$. The oxygen variations could reflect fractional crystallization ± crustal contamination, since the $\delta^{18}O$ variations are of the order of 1.17‰ (Taylor and Sheppard, 1986). On the other hand, Colima volcano data show a well-arranged negative correlation between the ε_{Nd} and $\delta^{18}O$ values (Fig. 11B), with a decrease in ε_{Nd} with increasing $\delta^{18}O$ values toward the Manzanillo and Jilotlán Batholiths, which confirms that crustal contamination took place.

CONCLUSIONS

Colima volcano is geochemically and isotopically characterized as the most primitive andesitic stratovolcano of the Mexican volcanic belt. In comparison to Nevado de Toluca, Popocatépetl, La Malinche, and Pico de Orizaba volcanoes, Colima volcano displays the lowest $^{87}Sr/^{86}Sr$ and $^{206}Pb/^{204}Pb$ ratios and most elevated ε_{Nd} values (Schaaf et al., 2004; Table 4). Although variations in these parameters can be interpreted as consequences of different contributions from the subducted slab, we emphasize the importance of lithologically different basement domains as an important factor in magma-generation processes beneath these volcanoes.

A characteristic feature of Colima volcano magmatic products is their homogeneous isotopic compositions for all four mea-

TABLE 4. COMPARISON OF SR-ND-PB ISOTOPIC DATA FROM FIVE MEXICAN VOLCANIC BELT STRATOVOLCANOES

Volcano	$^{87}Sr/^{86}Sr$	ε-Nd	$^{206}Pb/^{204}Pb$
Colima	0.7035–0.7036	+6.9 to +5.3	18.57–18.61
Toluca	0.7037–0.7042	+6.7 to +3.8	18.55–18.68
Popocatépetl	0.7040–0.7045	+6.2 to +2.5	18.62–18.78
Malinche	0.7046–0.7048	+2.0 to +0.8	18.59–18.63
Orizaba	0.7037–0.7048	+1.4 to –1.8	18.61–18.78

Note: Data from Schaaf et al. (2004).

sured systems (Sr, Nd, Pb, O). This suggests a relatively homogeneous magmatic source, but more analyses for prehistorical Colima volcano, Nevado de Colima, and Cántaro volcanoes are necessary to confirm this observation.

Colima volcano magmas were generated in a depleted mantle source and subsequently stored at crustal levels, where fractional crystallization was the most important magmatic process. During ascent, at higher-crustal levels, the magmas of Colima volcano were "contaminated" with Mesozoic gabbroic-granodioritic host rocks, comparable or identical to those of the Manzanillo and Jilotlán Batholiths, which display Sr and Nd isotope ratios similar to those of the Colima volcano andesites. The $\delta^{18}O$ values of Colima volcano and basement rocks differ substantially and show Colima volcano in an intermediate position between the surrounding primitive basalts from Jilotlán and the plutonic rocks (Fig. 11). This observation confirms that crustal contamination was important during the evolution of Colima volcano magmas, and it also shows that the O isotopic system is more sensitive with respect to these magmatic processes.

ACKNOWLEDGMENTS

This project was supported by CONACyT grant # 32330-T to P.S. Ricardo Saucedo, and Juan Carlos Gavilanes assisted during sample collection, and Nick Varley provided samples from the 2001 and 2002 domes. Diego Aparicio, Instituto de Geología, Universidad Nacional Autónoma de México (UNAM), helped during thin section preparation. Thanks are due to Rufino Lozano and Patricia Girón (Laboratorio Universitario de Geoquímica Isotópica [LUGIS]) for X-ray fluorescence analyses and to Gabriela Solís, María del Sol Hernández, Juan Morales, and Teodoro Hernández (LUGIS) for their assistance during sample preparation and isotope analyses. This contribution is part of the Ph.D. thesis of the first author and was financially supported by DGEP (Dirección General de Estudios de Posgrado) and CONACyT (Consejo Nacional de Ciencia y Tecnología) grants. Oxygen isotope analyses were performed under the COE21 Collaboration Program at the Institute for Study of the Earth's Interior (ISEI), Okayama University, Japan. Tazue Nogi (ISEI) helped with the oxygen isotope analyses. We give many thanks to Barbara Martiny and Gabriela Solís for their comments on earlier versions of the manuscript, and to James Allan and Jim Luhr for their constructive reviews.

REFERENCES CITED

Allan, J., 1986, Geology of the northern Colima and Zacoalco grabens, southwest Mexico: Late Cenozoic rifting in the Mexican volcanic belt: Geological Society of America Bulletin, v. 97, p. 473–485, doi: 10.1130/0016-7606(1986)97<473:GOTNCA>2.0.CO;2.

Allan, J., and Carmichael, I.S.E., 1984, Lamprophyric lavas in the Colima graben, SW Mexico: Contributions to Mineralogy and Petrology, v. 88, p. 203–216, doi: 10.1007/BF00380166.

Bandy, W., Mortera-Gutiérrez, C., Urrutia-Fucugauchi, J., and Hilde, T., 1995, The subducted Rivera-Cocos boundary: Where is it, what is it, and what is its relationship to the Colima rift: Geophysical Research Letters, v. 22, p. 3075–3078, doi: 10.1029/95GL03055.

Bindeman, I., Ponomareva, V., Bailey, J., and Valley, J., 2004, Volcanic arc of Kamchatka: A province with high-$\delta^{18}O$ magma sources and large-scale $^{18}O/^{16}O$ depletion of the upper crust: Geochimica et Cosmochimica Acta, v. 68, p. 841–865, doi: 10.1016/j.gca.2003.07.009.

Bretón-González, M., Ramírez, J.J., and Navarro, C., 2002, Summary of the historical eruptive activity of Volcan de Colima Mexico 1519–2000: Journal of Volcanology and Geothermal Research, v. 117, p. 21–46, doi: 10.1016/S0377-0273(02)00233-0.

Carmichael, I.S.E., 2002, The andesite aqueduct: Perspectives on the evolution of intermediate magmatism in west-central (105–99°W) Mexico: Contributions to Mineralogy and Petrology, v. 143, p. 641–663.

Carmichael, I.S.E., and DePaolo, D.J., 1980, Nd and Sr isotopes in the lavas of Colima, Mexico: Geological Society of America Abstracts with Programs, v. 12, p. 398.

Chivas, A., Andrew, A., Sinha, A., and O'Neil, J., 1982, Geochemistry of a Pliocene-Pleistocene oceanic-arc pluton complex, Guadalcanal: Nature, v. 300, p. 139–143, doi: 10.1038/300139a0.

Cortés-Cortés, A., Garduño-Monroy, V.H., Navarro, C., Komorowski, J.C., Saucedo, R., Macías, J.L., and Gavilanes, J.C., 2005, Geología del complejo volcánico de Colima: Serie de mapas del Instituto de Geología: Mexico City, Universidad Nacional Autónoma de México (in press).

Costa, F., Dungan, M., and Singer, B., 2002, Hornblende- and phlogopite- bearing gabbroic xenoliths from Volcán San Pedro (36°S), Chilean Andes: Evidence for melt and fluid migration and reactions in subduction-related plutons: Journal of Petrology, v. 43, p. 219–241, doi: 10.1093/petrology/43.2.219.

Cox, K., Bell, J., and Pankhurst, R., 1979, The interpretation of igneous rocks: London, George Allen & Unwin, 449 p.

De La Cruz-Reyna, S., 1993, Random patterns of occurrence of explosive eruptions at Colima Volcano, Mexico: Journal of Volcanology and Geothermal Research, v. 55, p. 51–68, doi: 10.1016/0377-0273(93)90089-A.

Eiler, J., Grönvold, K., and Kitchen, N., 2000, Oxygen isotope evidence for the origin of chemical variations in lavas from Theistareykir volcano in Iceland's northern volcanic zone: Earth and Planetary Science Letters, v. 184, p. 269–286, doi: 10.1016/S0012-821X(00)00318-6.

Gómez-Tuena, A., Langmuir, C., Goldstein, S., Lagatta, A., and Ortega-Gutiérrez, F., 2004, Chemically contrasting slab-derived fluxes in the Mexican volcanic belt (MVB) and their relation to the thermal structure of the Mexican subduction zone: International Geological Congress, Florence, Abstracts, p. 1028.

Hansteen, T., and Troll, V., 2003, Oxygen isotope composition of xenoliths from oceanic crust and volcanic edifice beneath Gran Canaria (Canary Islands): Consequences for crustal contamination of ascending magmas: Chemical Geology, v. 193, p. 181–193, doi: 10.1016/S0009-2541(02)00325-X.

Harris, C., and Bell, J., 1982, Natural partial melting of syenite blocks from Ascension Island: Contributions to Mineralogy and Petrology, v. 79, p. 107–113, doi: 10.1007/BF01132880.

Heliker, C., 1995, Inclusions in Mount St. Helens dacite erupted from 1980 through 1983: Journal of Volcanology and Geothermal Research, v. 66, p. 115–135, doi: 10.1016/0377-0273(94)00074-Q.

Hochstaedter, A., Ryan, J., Luhr, J., and Hasenaka, T., 1996, On B/Be ratios in the Mexican volcanic belt: Geochimica et Cosmochimica Acta, v. 60, p. 613–628, doi: 10.1016/0016-7037(95)00415-7.

James, D., 1981, The combined use of oxygen and radiogenic isotopes as indicators of crustal contamination: Annual Reviews of the Earth and Planetary Science Letters, v. 9, p. 311–344, doi: 10.1146/annurev.ea.09.050181.001523.

Kay, S., Mpodozis, C., and Coira, B., 1999, Magmatism, tectonism, and min-

eral deposits of the Central Andes (22°–35°S latitude), *in* Skinner, B., ed. Geology and ore deposits of the Central Andes: Society of Economic Geology Special Publication 7, p. 27–59.

Komorowski, J., Navarro, C., Cortés, A., Siebe, C., and Rodríguez, S., 1993, Multiple collapse of Volcán de Colima, Mexico, since 10,000 yr B.P.: Implications for eruptive style, magma yield, edifice stability and volcanic risk: International Association of Volcanology and Chemistry of the Earth's Interior, General Assembly, Canberra, Australia, Abstracts, p. 60.

Kusakabe, M., Maruyama, S., Nakamura, T., and Yada, T., 2004, CO_2 laser-BrF_5 fluorination technique for analysis of oxygen three isotopes of rocks and minerals: Journal of Mass Spectrometry Society of Japan, v. 52, p. 205–212.

Lassiter, J., and Luhr, J., 2001, Osmium abundance and isotope variations in mafic Mexican volcanic rocks: Evidence for crustal contamination and constraints on the geochemical behavior of osmium during partial melting and fractional crystallization: Geochemistry, Geophysics, Geosystems, v. 2, paper number 2000GC000116.

Luhr, J.F., 1997, Extensional tectonics and the diverse primitive volcanic rocks in the western Mexican volcanic belt: Canadian Mineralogist, v. 35, p. 473–500.

Luhr, J.F., 2002, Petrology and geochemistry of the 1991, 1998–1999 lava flows from the Volcán de Colima, Mexico: Implications for the end of the current eruptive cycle: Journal of Volcanology and Geothermal Research, v. 117, p. 169–194.

Luhr, J.F., and Carmichael, I.S.E., 1980, The Colima volcanic complex, Mexico. I. Post-caldera andesites from Volcán Colima: Contributions to Mineralogy and Petrology, v. 71, p. 343–372, doi: 10.1007/BF00374707.

Luhr, J.F., and Carmichael, I.S.E., 1982, The Colima volcanic complex, Mexico. III. Ash and scoria fall deposits from the upper slopes of Volcán Colima: Contributions to Mineralogy and Petrology, v. 80, p. 262–275, doi: 10.1007/BF00371356.

Luhr, J.F., and Carmichael, I.S.E., 1990, Geology of Volcán de Colima: Boletín del Instituto de Geología, Universidad Nacional Autónoma de México, no. 107, p. 101.

Luhr, J.F., and Prestegaard, K.L., 1988, Caldera formation at Volcán de Colima, Mexico, by a large Holocene volcanic debris avalanche: Journal of Volcanology and Geothermal Research, v. 35, p. 335–348, doi: 10.1016/0377-0273(88)90027-3.

Macías, J., Capaccioni, B., Conticelli, S., Giannini, M., Martini, M., and Rodríguez, S., 1993, Volatile elements in alkaline and calc-alkaline rocks from the Colima graben, Mexico: Constraints on their genesis and evolution: Geofísica Internacional, v. 32, p. 575–589.

McBirney, A.R., Taylor, H.P., and Armstrong, R.L., 1987, Paricutin re-examined: A classic example of crustal assimilation in calc-alkaline magma: Contributions to Mineralogy and Petrology, v. 95, p. 4–20, doi: 10.1007/BF00518026.

McLennan, S., Taylor, S., McCulloch, M., and Maynard, J., 1990, Geochemical and Sr-Nd isotopic composition of deep-sea turbidites: Crustal evolution and plate tectonic associations: Geochimica et Cosmochimica Acta, v. 54, p. 2015–2050, doi: 10.1016/0016-7037(90)90269-Q.

Medina, F., 1983, Analysis of the eruptive history of the Volcán de Colima, Mexico (1560–1980): Geofísica Internacional, v. 22, p. 157–178.

Moorbath, S., Thorpe, R., and Gibson, I., 1978, Strontium isotope evidence for petrogenesis of Mexican andesites: Nature, v. 271, p. 437–439, doi: 10.1038/271437a0.

Mora, J.C., Macías, J.L., Saucedo, R., Orlando, A., Manetti, P., and Vaselli, O., 2002, Petrology of the 1998–2000 products of Volcán de Colima, México: Journal of Volcanology and Geothermal Research, v. 117, p. 195–212, doi: 10.1016/S0377-0273(02)00244-5.

Nixon, G.T., 1988, Petrology of the younger andesites and dacites of Iztaccíhuatl volcano, Mexico: II. Chemical stratigraphy, magma mixing, and the composition of basaltic magma influx: Journal of Petrology, v. 29, p. 265–303.

Pardo, M., and Suárez, G., 1995, Shape of the subducted Rivera and Cocos plates in southern Mexico: Seismic and tectonic implications: Journal of Geophysical Research, v. 100, p. 12,357–12,373, doi: 10.1029/95JB00919.

Robin, C., Komorowski, J.C., Boudal, C., and Mossand, P., 1990, Evidence of magma mixing in juvenile fragments from pyroclastic surge deposits associated with debris avalanche deposits at Colima volcanoes, Mexico: Bulletin of Volcanology, v. 52, p. 391–403, doi: 10.1007/BF00302051.

Robin, J., and Potrel, A., 1993, Multi-stage magma mixing in the pre-caldera series of Fuego de Colima volcano: Geofísica Internacional, v. 32, p. 605–615.

Robin, J., Mossand, P., Camus, G., Cantagrel, J.M., Gourgaud, A., and Vincent, P.M., 1987, Eruptive history of the Colima volcanic complex (Mexico): Journal of Volcanology and Geothermal Research, v. 31, p. 99–113, doi: 10.1016/0377-0273(87)90008-4.

Robin, J., Camus, G., and Gourgaud, A., 1991, Eruptive cycles at Fuego de Colima volcano (México): Journal of Volcanology and Geothermal Research, v. 45, p. 209–225, doi: 10.1016/0377-0273(91)90060-D.

Rodríguez-Elizarrarás, S., 1995, Estratigrafía y estructura del Volcán de Colima, México: Revista Mexicana de Ciencias Geológicas, v. 12, p. 22–46.

Rodríguez-Elizarrarás, S., Siebe, C., Komorowski, J., Espíndola, J., and Saucedo, R., 1991, Field observations of pristine block and ash flow deposits emplaced April 16–17, 1991 at Volcán de Colima, Mexico: Journal of Volcanology and Geothermal Research, v. 48, p. 399–412, doi: 10.1016/0377-0273(91)90054-4.

Saucedo, R., 1997, Reconstrucción de la erupción de 1913 del Volcán de Colima [M.S. thesis]: Mexico City, Posgrado en Ciencias de la Tierra, Universidad Nacional Autónoma de México, 185 p.

Saucedo, R., and Macías, J.L., 1999, La historia del volcán de Colima: Tierra Adentro, v. 98, p. 8–14.

Saucedo, R., Macías, J., Bursik, M., Mora, J., Gavilanes, J., and Cortés, A., 2002, Emplacement of pyroclastic flows during the 1998–1999 eruption of Volcán de Colima, Mexico: Journal of Volcanology and Geothermal Research, v. 117, p. 129–153, doi: 10.1016/S0377-0273(02)00241-X.

Saucedo, R., Macías, J., and Bursik, M., 2004, Pyroclastic flow deposits of the 1991 eruption of Volcán de Colima, México: Bulletin of Volcanology, v. 66, p. 291–306, doi: 10.1007/s00445-003-0311-0.

Schaaf, P., 1990, Isotopengeochemische Untersuchungen an granitoiden Gesteinen eines aktiven Kontinentalrandes: Alter und Herkunft der Tiefengesteinskomplexe der Pazifikküste Mexikos, zwischen Puerto Vallarta und Acapulco [Ph.D. thesis]: Münich, University of Münich, 202 p.

Schaaf, P., Martínez-Serrano, R., Siebe, C., Macías, J.L., Carrasco, G., Castro, R., and Valdez, G., 2004, Heterogeneous magma compositions of Trans-Mexican volcanic belt stratovolcanoes—Geochemical and isotopic evidence for different basement compositions, *in* Aguirre, G., Macías, J.L., and Siebe, C., eds., Neogene-Quaternary continental margin volcanism: Proceedings of the Geological Society or America Penrose Conference, Publicación Especial, Instituto de Geología, Universidad Nacional Autónoma de México, p. 68.

Schaaf, P., Stimac, J., Siebe, C., and Macías, J.L., 2005, Geochemical evidence for mantle origin and crustal processes in volcanic rocks from Popocatépetl and surrounding monogenetic volcanoes, central Mexico: Journal of Petrology, v. 46, p. 1243–1282, doi: 10.1093/petrology/egi015.

Smith, S.A., 1990, A geologic reconnaissance study of a Middle Cretaceous marine volcanic arc: The stratigraphic evolution and subsequent strike-slip fragmentation of the Colima basin [M.S. thesis]: New Orleans, Louisiana, University of New Orleans, 70 p.

Smithsonian Institution, 2002, Bulletin of Global Volcanism Network, v. 27, no. 5 (online).

Sun, S., and McDonough, W., 1989, Chemical and isotopic systematics of oceanic basalts: Implications for mantle compositions and processes, *in* Saunders, A., and Norry, M., eds., Magmatism in ocean basins: Geological Society [London] Special Publication 42, p. 313–345.

Taran, Y., Kusakabe, M., Mora, J.C., and Valdez, G., 2002, Hydrogen isotopic composition of hornblendes from active volcanoes of Mexico: Implication for origin of magmatic water: GEOS, v. 22, p. 261.

Taylor, H.P., Jr., 1980, The effects of assimilation of country rocks by magmas on $^{18}O/^{16}O$ and $^{87}Sr/^{86}Sr$ systematics in igneous rocks: Earth and Planetary Science Letters, v. 47, p. 243–254, doi: 10.1016/0012-821X(80)90040-0.

Taylor, H., Jr., and Sheppard, S., 1986, Igneous rocks: I. Processes of isotopic fractionation and isotope systematics, *in* Valley, J., Taylor, H., Jr., and O'Neil, J., eds., Stable isotopes in high temperature geological processes: Mineralogical Society of America Reviews in Mineralogy, v. 16, p. 227–271.

Urrutia-Fucugauchi, J., and Molina-Garza, R., 1992, Gravity modelling of regional crustal and upper mantle structure of Guerrero terrane. 1. Colima graben and southern Sierra Madre Occidental, western Mexico: Geofísica Internacional, v. 31, p. 493–507.

Urrutia-Fucugauchi, J., Flores-Ruíz, J., Bandy, W., and Mortera-Gutierrez, C., 1999, Crustal structure of Colima rift, western Mexico: Gravity models revisited: Geofísica Internacional, v. 38, p. 205–216.

Verma, S., 2000, Geochemistry of the subducting Cocos plate and the origin of subduction-unrelated mafic volcanism at the volcanic front of the central Mexican volcanic belt, *in* Delgado-Granados, H., Aguirre-Díaz, G., and

Stock, J, M., eds., Cenozoic tectonics and volcanism of Mexico: Geological Society of America Special Paper 334, p. 195–222.

Verma, S., and Luhr, J.F., 1993, Sr-Nd-Pb isotope and trace element geochemistry of calc-alkaline andesites from Volcán Colima, Mexico: Geofísica Internacional, v. 32, p. 617–631.

Vroon, P., Lowry, D., Van Bergen, M., Boyce, A., and Mattey, D., 2001, Oxygen isotope systematics of the Banda Arc: Low $\delta^{18}O$ despite involvement of subducted continental material in magma genesis: Geochimica et Cosmochimica Acta, v. 65, p. 589–609, doi: 10.1016/S0016-7037(00)00554-8.

Wallace, P., and Carmichael, I., 1994, Petrology of Volcán Tequila, Jalisco, Mexico: Disequilibrium phenocryst assemblages and evolution of the subvolcanic magma system: Contributions to Mineralogy and Petrology, v. 117, p. 345–361, doi: 10.1007/BF00307270.

Wilcox, R.E., 1954, Petrology of Paricutín volcano, México: U.S. Geological Survey Bulletin, v. 965C, p. 281–353.

Manuscript Accepted by the Society 28 July 2005

Printed in the USA